# Molecular Insight into the Liquid Propan-2-ol + Water Mixture

Y. Mauricio Muñoz-Muñoz, Gabriela Guevara-Carrion, and Jadran Vrabec*

*Thermodynamics and Energy Technology, University of Paderborn, 33098 Paderborn, Germany*

E-mail: jadran.vrabec@upb.de

Phone: +49 5251 60-2420

**Abstract**

The hydrogen bonding structure of the mixture water + propan-2-ol is analyzed at ambient conditions of temperature and pressure with molecular modeling and simulation techniques. A new force field for propan-2-ol is developed for this purpose on the basis of quantum chemical calculations and validated for a wide range of macroscopic properties. The basic mixing properties excess volume and excess enthalpy as well as the most important transport properties, i.e. diffusion coefficients and shear viscosity, are considered to verify the suitability of the employed force fields for studying the complex behavior of this aqueous alcoholic mixture. Radial distribution functions and hydrogen bonding statistics are employed to characterize the hydrogen bond network and molecular clustering. Inhomogeneous mixing on the microscopic level, given by the presence of segregation pockets, is identified. The interrelation between the intriguing macroscopic behavior of this binary mixture and its microscopic structure is revealed.

# Introduction

Mixtures of water and an amphiphilic solute, such as an alcohol, exhibit thermodynamic and transport properties that differ significantly from values that are expected for an ideal liquid mixture. Their behavior is governed by the strong tendency of the involved molecules to form organized structures due to the presence of hydrophobic regions which aggregate the hydrophilic groups, facilitating hydrogen bonding with the surrounding water molecules[1].

Aqueous alcoholic mixtures have been extensively investigated by experimental and theoretical approaches due to their importance in life sciences and numerous industrial processes, like electron transfer reactions, heterogeneous catalysis or fuel cell technology[2,3]. However, there is still no consensus on the microscopic factors that cause the anomalous behavior of their macroscopic properties. The classical explanation based on hydrophobic hydration, that is attributed to the presence of enhanced clathrate-like water structures[4], was challenged by diffraction experiments[1,5] and issues concerning clustering, molecular segregation and microheterogeneity have

gained relevance[6–9].

Molecular modeling and simulation has become an important avenue for investigating the microscopic details of hydrogen bonding structures[10], which are hardly or not accessible at all with experimental techniques[11]. It has also been successfully employed to explain macroscopic phenomena[12] or to interpret spectroscopic data[13] from a microscopic point of view. The present work aims at a deeper understanding of the thermodynamic properties and unique microscopic structural dynamics of aqueous alcoholic mixtures by means of molecular modeling and simulation. While aqueous mixtures of methanol and ethanol have been investigated in preceding work[14], the present contribution focuses on propan-2-ol, which is the largest secondary alcohol that is fully miscible in water. It is present in many commercial products, such as disinfectants, paint and ink formulations, fuel additives or de-icer products[15]. Further, the aqueous propan-2-ol mixture has throughly been investigated with a wide variety of experimental techniques[5,7,9,15–18].

Numerous molecular simulation studies were presented for aqueous alcoholic mixtures[13,15,19–23], sometimes leading to apparently contradictory results[1]. A possible cause may be the force field selection. For instance, Gereben and Pusztai[13] found a significant variation with respect to coordination number, hydrogen bonding and spatial distribution for aqueous ethanol depending on different water force fields. Nonetheless, in most literature work, the underlying force fields were not adequately validated, e.g., only time-independent properties were considered and the dynamic behavior was neglected.

The reliability of molecular simulation is determined by the employed force fields, i.e. a mathematical representation of the molecular interactions. There has thus been a continuous effort with respect to the development of force fields that are able to cover a wide variety of physical properties[24–26], employing, among others, quantum chemical calculations. In this work, a rigid non-polarizable force field for propan-2-ol (CAS-Number 67-63-0, or henceforth IPA) was developed, which was optimized to experimental vapor-liquid equilibrium (VLE) and transport coefficient data following a procedure that is similar to the one outlined in Ref.[27]. This force field was tested together with the well-known TIP4P/2005 water force field[28] on its ability to predict macroscopic

excess and transport properties of their mixture at ambient conditions of temperature and pressure. Further, the local ordering of water and propan-2-ol molecules and the structure of the hydrogen bond network was examined. For this purpose, radial distribution functions (RDF) were sampled in the entire composition range and compared with those of the pure constituent substances. Because of the key role of hydrogen bonding for the understanding of the microscopic structure and dynamical properties of aqueous solutions[23], the RDF were carefully analyzed.

Excess properties are important quantities to describe the extent of mixture non-idealitiy. Transport properties are strongly affected by the presence of organized microstructures, which are a consequence of molecular association due to hydrogen bonding. It is well known that aqueous alcoholic mixtures contain long-lived clusters[29]. Thus, it is expected that force fields that are able to adequately predict properties such as excess volume, shear viscosity or diffusion coefficients do yield trustworthy structural information on the molecular level.

Recently, Bye et al.[15] studied the mesoscopic structure of propan-2-ol + water with perturbation calorimetry and molecular simulation employing the TIP3P force field for water and the amber gaff03 force field for the alcohol. They calculated hydrogen bonding statistics and a non-ideality degree. However, the authors did not indicate whether the employed force field combination is capable to yield mixture density or other thermodynamic properties appropriately. Anisimov et al.[20] obtained RDF and dipole distributions of aqueous propan-2-ol, employing polarizable force fields based on the Drude model. They successfully tested their propan-2-ol force field for the self-diffusion coefficient of the pure substance, however, the time-independent properties of the mixture were not assessed.

This paper is organized as follows: First, theoretical background and methodology are described. Second, a new propan-2-ol force field is introduced and validated, followed by a description of its microscopic structure. Subsequently, simulation results for the excess and transport properties of the mixture are compared with the available experimental data. RDF and hydrogen bonding statistics are interpreted in the light of the microscopic structure of aqueous propan-2-ol. Snapshots of molecular configuration are also considered. Finally, conclusions are drawn. Com-

putational details and numerical results are given in the supplementary material.

# Theory and Methodology

Several approaches to define a hydrogen bond, based on energetic[30], geometric[31] or topological[32] criteria, can be found in the literature. Because there is still no exact definition, geometric criteria are employed in most cases. Accordingly, molecules were considered to form a hydrogen bond in this work if the following conditions hold[33]:

- The distance between the donor and the acceptor $\ell_{\mathrm{AD}}$ is smaller than a threshold distance.
- The distance between the acceptor sites of the acceptor and donor molecules $\ell_{\mathrm{AA}}$ is smaller than a threshold distance.
- The angle between the acceptor–donor axis and the acceptor–acceptor axis is smaller than a threshold angle $\varphi_{\mathrm{DAA}}$.

Threshold values proposed by Haughney et al.[31] ($\ell_{\mathrm{AD}}$ = 2.6 Å, $\ell_{\mathrm{AA}}$ = 3.5 Å and $\varphi_{\mathrm{DAA}} = 30^{\circ}$) were employed in this work.

Transport coefficients were sampled with equilibrium molecular dynamics and the Green-Kubo formalism[34,35]. This formalism was preferred over non-equilibrium methods because it can simultaneously yield several transport coefficients. The self-diffusion coefficient $D_i$, also termed as intra-diffusion coefficient in the case of mixtures, the Maxwell-Stefan (MS) diffusion coefficient $Đ$ and the shear viscosity $\eta$ were sampled concurrently.

Fick's law and Maxwell-Stefan (MS) theory are the most popular approaches to describe transport diffusion in mixtures, relating the molar flux to a driving force. Fick's law assumes the mole fraction gradient $\nabla x_j$, a quantity that is measurable in the laboratory, whereas MS theory expresses the driving force in terms of the chemical potential gradient $\nabla \mu_i$[36].

The MS approach accounts for thermodynamics and mass transfer separately, such that only the latter contribution is characterized by the MS diffusion coefficient $Đ$. Because $Đ$ is related to

the chemical potential gradient, it cannot be measured in the laboratory directly. However, the MS diffusion coefficient can well be sampled by molecular dynamics simulation. The starting point are the Onsager phenomenological coefficients $L_{ij}$[37]

$$L_{ij} = \frac{1}{3N} \int_0^\infty dt \left\langle \sum_{k=1}^{N_i} \mathbf{v}_i^k(0) \cdot \sum_{l=1}^{N_j} \mathbf{v}_j^l(t) \right\rangle, \tag{1}$$

where $\mathbf{v}_i^k(t)$ is the center of mass velocity vector of molecule $k$ of component $i$ at some time $t$, $N_i$ is the number of molecules of component $i$ and $N$ is the total number of molecules. The brackets $<...>$ denote the canonic $NVT$ ensemble average. The MS diffusion coefficient for a binary mixture is then given by[37]

$$Đ = \frac{x_j}{x_i} L_{ii} + \frac{x_i}{x_j} L_{jj} - L_{ij} - L_{ji} \cdot \tag{2}$$

The thermodynamic contribution is considered by the so-called thermodynamic factor $\Gamma$

$$\Gamma = 1 + x_1 \left( \frac{\partial \ln \gamma_1}{\partial x_1} \right)_{T,p} = 1 + x_2 \left( \frac{\partial \ln \gamma_2}{\partial x_2} \right)_{T,p}, \tag{3}$$

where $\gamma_i$ stands for the activity coefficient of component $i$. Fick and MS diffusion coefficients describe the same phenomenon on so that they can be converted into each other by

$$D = Đ \cdot \Gamma, \tag{4}$$

in the case of a binary mixture. For the calculation of the thermodynamic factor, the composition dependence of the activity coefficients is required. Following the Gibbs-Duhem equation, the excess Gibbs energy $G^{\mathrm{E}}$ of the binary mixture is related to the individual activity coefficients by[38]

$$k_B T \ln \gamma_1 = \left( \frac{\partial G^{\mathrm{E}}}{\partial n_1} \right)_{T,p} \text{ and } \; k_B T \ln \gamma_2 = \left( \frac{\partial G^{\mathrm{E}}}{\partial n_2} \right)_{T,p}, \tag{5}$$

where $n_i$ is the number of moles of component $i$ in the mixture. Therefore, a mathematical expression for $G^{\mathrm{E}}$ as a function of mole fraction is needed to calculate the thermodynamic factor

from Eq. (5). In this work, binary parameters of the classical Wilson[39] $G^{\mathrm{E}}$ model were regressed to experimental VLE data[40]. The composition derivatives of the Wilson model were evaluated analytically as described by Taylor and Kooijman[41] to determine the thermodynamic factor.

The self- and intra-diffusion coefficients can be sampled on the basis of the individual molecule velocity autocorrelation functions

$$D_i = \frac{1}{3N_i} \int_0^\infty dt \, \left\langle \mathbf{v}_i^k(t) \cdot \mathbf{v}_i^k(0) \right\rangle \cdot \tag{6}$$

The shear viscosity $\eta$ is associated with the off-diagonal elements of the microscopic stress tensor $J_p^{xy}$

$$\eta = \frac{1}{V k_B T} \int_0^\infty dt \, \left\langle J_p^{xy}(t) \cdot J_p^{xy}(0) \right\rangle, \tag{7}$$

where $V$ stands for the volume and

$$J_p^{xy} = \sum_{k=1}^{N} m_k v_k^x v_k^y - \frac{1}{2} \sum_{k=1}^{N} \sum_{l \neq k}^{N} r_{kl}^x \frac{\partial u(r_{kl})}{\partial r_{kl}^y}. \tag{8}$$

Here, $k$ and $l$ denote different molecules of any species. The upper indices $x$ and $y$ stand for the spatial vector components, e.g. for velocity $v_k^x$ or site-site distance $r_{kl}^x$. Eqs. (7) and (8) may directly be applied to mixtures. Five independent terms of the stress tensor $J_p^{xy}$, $J_p^{xz}$, $J_p^{yz}$, $(J_p^{xx} - J_p^{yy})/2$ and $(J_p^{yy} - J_p^{zz})/2$ were considered to improve statistics[42].

Finite-size effects on the sampled diffusion coefficients were corrected with the approach of Yeh and Hummer[43] for the intra-diffusion coefficients and by Jamali et al.[44] for the Fick diffusion coefficients. The finite-size corrections are between 3 and 7% of the simulation results for the intradiffusion coefficients and between 6 and 15% for the Fick diffusion coefficients. No significant finite-size effects are expected for the shear viscosity calculation[45–47], thus no corrections were made.

# Propan-2-ol Force Field

The present force field for propan-2-ol is rigid, non-polarizable and of united-atom type. It consists of four LJ sites and three point charges, two of which are located on the hydroxyl group and the third one is at the center of the methanetriyl site (–CH<). The potential energy $u_{ij}$ between two molecules $i$ and $j$ is thus

$$u_{ij}\left(r_{ijab}\right) = \sum_{a=1}^{S_i^{\mathrm{LJ}}} \sum_{b=1}^{S_j^{\mathrm{LJ}}} 4\varepsilon_{ab} \left[ \left( \frac{\sigma_{ab}}{r_{ijab}} \right)^{12} - \left( \frac{\sigma_{ab}}{r_{ijab}} \right)^{6} \right] + \sum_{c=1}^{S_i^{\mathrm{e}}} \sum_{d=1}^{S_j^{\mathrm{e}}} \frac{1}{4\pi\varepsilon_0} \frac{q_{ic} q_{jd}}{r_{ijcd}}, \tag{9}$$

where $a$ is the site index of molecule $i$ and $b$ the site index of molecule $j$. $S_i$ and $S_j$ are the number of interaction sites of molecules $i$ and $j$, respectively. $r_{ijab}$ represents the site-site distance between molecules $i$ and $j$. The LJ size and energy parameters are $\sigma_{ab}$ and $\varepsilon_{ab}$, which were specified according the Lorentz-Berthelot combination rules for the binary mixture, i.e. $\sigma_{ab} = (\sigma_{aa} + \sigma_{bb})/2$ and $\varepsilon_{ab} = \sqrt{\varepsilon_{aa}\varepsilon_{bb}}$. $q_{ic}$ and $q_{jd}$ are point charges located at sites $a$ and $b$ on the molecules $i$ and $j$, whereas $\varepsilon_0$ is the permittivity of vacuum.

The geometric parameters, i.e. bond lengths and internal angles, as well as the magnitudes of the point charges were taken from the quantum chemical data base of the National Institute of Standards and Technology (NIST)[48]. The model parameters were obtained with an optimization procedure that was reported in prior works[26,27], i.e. the $Z$ matrix[49] of propan-2-ol was calculated to obtain bond lengths as well as the angles $\theta_{i,j,k}$ between three and $\phi_{i,j,k,l}$ between four successive sites. All angles, the LJ parameters of the oxygen and methanetriyl sites as well as the magnitude of the point charges were kept constant during the fitting procedure. The LJ parameters of the methyl sites $\varepsilon_{\mathrm{CH3}}$ and $\sigma_{\mathrm{CH3}}$ as well as the site-site bond lengths were simultaneously optimized in an iterative process with Monte Carlo and equilibrium molecular dynamics simulations to reproduce experimental VLE and transport coefficient data. The resulting propan-2-ol force field parameters are listed in Table 1.

[0]Footnote

**Table 1: Present force field parameters for propan-2-ol, where $x$, $y$, $z$ stand for the site positions.**

| site | $x$/Å | $y$/Å | $z$/Å | $\varepsilon/k_B$/K | $\sigma$/Å | $q$/e |
|---|---|---|---|---|---|---|
| $CH_3$ | -1.109 | 2.128 | -1.265 | 103.59 | 3.866 | 0 |
| $CH_3$ | -3.081 | 1.135 | 0.077 | 103.59 | 3.866 | 0 |
| CH | -1.552 | 1.344 | 0 | 20.20 | 3.238 | 0.310 |
| O | -0.969 | 0 | 0 | 85.90 | 3.154 | -0.747 |
| H | 0 | 0 | 0 | 0 | 0 | 0.437 |

## Force Field Validation

Several important thermodynamic properties were sampled and compared with experimental literature data to validate the present force field. Vapor-liquid equilibrium including critical point, second virial coefficient, shear viscosity and self-diffusion coefficient are in excellent agreement with experimental data, cf. Fig. 1 and Fig. 2.

The average relative deviations of the saturated liquid density, vapor pressure and enthalpy of vaporization with respect to DIPPR correlations values[57] are 0.4%, 7.0% and 4.8%, respectively. These relative deviations are lower than those of the OPLS force field[58] between 400 K and 500 K, i.e. 4.3%, 16.1% and 32.9%, and those of the TraPPE-UA force field[59] between 300 K and 490 K, i.e. 4.8%, 20.3% and 7.4%. A graphical comparison of the VLE results can be found in supplementary information.

The predicted critical point by the present force field is $T_c = 504.2$ K, $p_c = 4.43$ MPa and $\rho_c = 4.44$ mol $l^{-1}$, showing an underestimation with respect to experimental data[60,61] of -0.8%, -7.0% and -1.4%, respectively. The OPLS force field exhibits deviations for the critical density, pressure and temperature of 4 to 5%, respectively[58] and the TraPPE-UA force field -1.2% and 3.8% for the critical temperature and critical density, respectively[59]. The second virial coefficient, which is strictly a pair-potential property[62], agrees with the experimental data in the entire temperature range. Note that the DIPPR correlation deviates considerably for temperatures above $\sim$ 800 K, cf. Fig. 1 (d). The numerical data are given in the supplementary information.

Transport properties in the homogeneous liquid range of states were sampled to obtain an

insight on the capability of the molecular model to cover the dynamic behavior of the alcohol. Both self-diffusion coefficient and shear viscosity are in excellent agreement with experimental data, cf. Fig. 2. For instance, the average relative deviation of the self-diffusion coefficient from the experimental values[68] is only 2.6% in the studied temperature range. Note that many force fields have problems to accurately predict both self-diffusion coefficient and density at a time, for instance, the OPLS and OPLS–AA force fields seriously overestimate the experimental self-diffusion coefficients[70]. Further, force fields that have been parameterized to fit self-diffusion coefficient may not reproduce the density adequately. A graphical comparison of the results for liquid density and self-diffusion coefficient from the present work and other force fields from the literature[71] can be found in supplementary information.

It should be noted that the velocity autocorrelation function (VACF) of liquid propan-2-ol has an exceptionally long tail, indicating velocity persistence[72], cf. supplementary information. In fact, in order to sample the self-diffusion coefficient of propan-2-ol under ambient conditions appropriately, a VACF of at least 250 ps was needed. This is in marked contrast to the 10 to 20 ps that are required for other short monohydroxyl alcohols like methanol or ethanol. In their classical paper, Alder and Wainwright[72] related the long-time tail of the VACF to the presence of vortex back-flow and ring collisions occurring over long (microscopic) time scales. At short times, alcohol molecules are surrounded by their solvation shell and when this local equilibrium is disturbed, the solvation shell has to rearrange and the hydroxyl groups have to find appropriate partners for a new hydrogen bonding configuration. Here, it is presumed that the slow loss of memory of the system is due to the relatively long time required for the steric screening[17] of the hydrophilic group induced by the bulky molecular geometry of propan-2-ol.

## Microstructure of Pure Propan-2-ol

The local structure of liquid propan-2-ol was studied by means of RDF at temperatures between 278.15 K and 338.15 K, cf. Fig. 3. As expected, a behavior that is typical for hydrogen bonding liquids was found, e.g. $g_{\mathrm{O-H}}(r)$ has a pronounced first peak located at $\sim$1.9 Å, indicating the

presence of a local structure at short site-site distances. The first peak of $g_{\mathrm{O-O}}(r)$ is located at $\sim$2.8 Å which corresponds to the literature value of 2.87 $\pm$ 0.1 Å obtained from X-ray scattering data[16]. This peak to is smaller than that of the corresponding $\mathrm{O-H}$ interactions and suggests preferential interactions at short site-site distances between the oxygen and hydrogen sites. Further, the magnitude of the first peaks of $g_{\mathrm{O-O}}(r)$ and $g_{\mathrm{O-H}}(r)$ decreases with temperature by about 20% in the regarded temperature range of 60 K, indicating thermally induced weakening of the hydrogen bonding structure. The broad peak at $\sim$ 4.7 Å represents the $\mathrm{O}\cdots\mathrm{O}$ interactions for the second neighbors in a hydrogen bonded alcohol chain and its observed in experimentally based RDF at $\sim$4.5 Å[16].

The average number of hydrogen bonds per propan-2-ol molecule is given by

$$\langle n_{\mathrm{O-H}} \rangle \simeq 4\pi\rho \left[ \int_0^{r_m^{\mathrm{O-H}}} r^2 g_{\mathrm{O-H}}(r) dr + \int_0^{r_m^{\mathrm{H-O}}} r^2 g_{\mathrm{H-O}}(r) dr \right], \tag{10}$$

where $\rho$ is the bulk density. The first integral in Eq. (10) corresponds to the number of hydrogen sites surrounding an oxygen site and the second one to the number of oxygen sites surrounding a hydrogen site inside the first coordination shells with radii $r_m^{\mathrm{O-H}}$ and $r_m^{\mathrm{H-O}}$, respectively. The average number of hydrogen bonds per propan-2-ol molecule is $\langle n_{\mathrm{O-H}} \rangle \approx 2$ at 278.15 K, which decreases monotonically with increasing temperature, yielding a total decay of 8% at 338.15 K. Further, present results suggest strong fluctuations of the local density at short intermolecular distances. E.g. at 278.15 K, $\rho(r)$ shows a maximum value of 25.7 mol $\mathrm{l}^{-1}$ at $\sim$4.6 Å and a minimum value of 9.2 mol $\mathrm{l}^{-1}$ at $\sim$7.5 Å. At 338.15 K, the local density has a maximum value of 22.5 mol $\mathrm{l}^{-1}$ at $\sim$4.6 Å and a minimum value of 9.2 mol $\mathrm{l}^{-1}$ at $\sim$7.5 Å. The local density reaches its bulk value only at large intermolecular distances >17 Å for both temperatures.

The extension of the hydrogen bond structure in liquid propan-2-ol was quantified on the basis of the geometric criterion[31,33] discussed above. At ambient conditions of temperature and pressure, around 77% of propan-2-ol molecules form trimers of linearly hydrogen bonded chains, i.e. they have two hydrogen bonds, which is in line with experimental results[73]. Further, the hydrogen bonding behavior of propan-2-ol is similar to that observed for methanol and ethanol. The resulting

hydrogen bonding statistics for propan-2-ol together with those for methanol and ethanol are listed in Table 2.

**Table 2: Fraction of alcohol molecules involved in hydrogen bonds (HB) at 298.15 K and 0.1 MPa.**

| No. of HB | 0 | 1 | 2 | 3 | 4+ | Force field |
|---|---|---|---|---|---|---|
| methanol | 0.0166 | 0.1593 | 0.7681 | 0.0560 | 0.0000 | [74] |
| ethanol | 0.0211 | 0.2025 | 0.6955 | 0.0817 | 0.0002 | [75] |
| propan-2-ol | 0.0110 | 0.1540 | 0.7701 | 0.0650 | 0.0002 | this work |

# Water + Propan-2-ol

## Excess Volume and Excess Enthalpy

Excess volume and excess enthalpy are basic mixing properties. In case of aqueous propan-2-ol, the non-ideal mixing effects are significant, cf. Fig. 4. Present simulations predict a minimum of the excess volume at around $x_{\mathrm{IPA}} = 0.4$ mol mol$^{-1}$, which is in good agreement with experimental literature data[63,76–79]. Near that minimum, a less pronounced (negative) excess volume was predicted with a deviation of about 10%. This accuracy was unexpected because relatively small excess volume values are difficult to predict[14].

The Redlich-Kister correlation was fitted to present results for the excess enthalpy and is shown together with experimental literature data[79–83] in Fig. 4 (bottom), its constants are listed in the supplementary material. It can be seen that the presence of a maximum (endothermic mixing) and a minimum (exothermic mixing) of the excess enthalpy was predicted. The exothermic mixing peak is located at an alcohol mole fraction of $x_{\mathrm{IPA}} \simeq 0.12$ mol mol $^{-1}$, which is near the experimental value $x_{\mathrm{IPA}} \simeq 0.09$ mol mol$^{-1}$. However, the endothermic mixing peak from molecular simulation, located at $x_{\mathrm{IPA}} \simeq 0.9$ mol mol$^{-1}$, is relatively far from the experimental data, $x_{\mathrm{IPA}} \simeq 0.7$ mol mol$^{-1}$. There is thus only a qualitative agreement between simulation and experiment, which is not surprising, as discussed in other simulation work on aqueous methanol and ethanol mixtures[14,84–88].

Hence, the quantitative prediction of the excess enthalpy of aqueous alcohol mixtures by molecular modeling and simulation remains a challenge.

## Thermodynamic Factor and Mutual Diffusion Coefficient

It has been shown for a wide variety of binary mixtures[89] that the Wilson model yields the most convincing results when compared to other $G^{\mathrm{E}}$ models for the evaluation of the thermodynamic factor. Nonetheless, the quality of the underlying experimental VLE data is crucial for an adequate estimation of the thermodynamic factor and only consistent VLE data should be employed for the adjustment of Wilson model parameters. Here, the VLE data set with the largest number of measured data points at 298.15 K[40] was employed and its consistency was confirmed by applying point to point[90,91] and area tests[92,93].

As can be seen in Fig. 5 (a), the thermodynamic factor has a minimum with a magnitude of $\Gamma = 0.22$ at $x_{\mathrm{IPA}} \simeq 0.3$ mol mol$^{-1}$, which is relatively close to the phase stability limit $\Gamma = 0$[97].

The Fick diffusion coefficient was calculated from the MS diffusion coefficient sampled by equilibrium molecular dynamics simulation and the thermodynamic factor based on experimental VLE data as described above. As can be seen in Fig. 5 (b), the strong composition dependence of the Fick diffusion coefficient is introduced by the thermodynamic factor, i.e. the minimum of the thermodynamic factor corresponds to the Fick diffusion coefficient minimum. Further, the present approach leads to a convincing prediction of the Fick diffusion coefficient in the entire composition range. The qualitative and quantitative agreement with experimental literature data is very good, especially at the water-rich region. Several diverging experimental data points for the Fick diffusion coefficient between $x_{\mathrm{IPA}} \simeq 0.7$ and 0.9 mol mol$^{-1}$ are the consequence of artifacts due to the presence of extrema in the refractive index[94], which make this concentration region difficult to access experimentally.

**Intra-diffusion Coefficient**

Random propagation of molecules is strongly affected by hydrogen bonding. As expected, the predicted intra-diffusion coefficient of propan-2-ol is lower than that of water, i.e. bulky propan-2-ol molecules propagate slower than the smaller water molecules cf. Fig. 5 (c). Further, the intra-diffusion coefficients of water and 2-propanol in their mixture show an initial strong decay in this region. In fact, water reduces its mobility by approximately 50% when the propan-2-ol mole fraction has merely reached $x_{\mathrm{IPA}} = 0.1$ mol mol$^{-1}$. At equimolar composition, water intra-diffusion is only one third of its original value. This strong reduction of water mobility is comparable to that observed for the water + ethanol mixture[14] and is a consequence of strongly attractive solute-solvent interactions[98]. When propan-2-ol is added to water, the probability of hydrogen bond formation between water and the alcohol increases, reducing water mobility. However, this effect does not persist in the entire composition range, i.e. water intra-diffusion increases at $x_{\mathrm{IPA}} > 0.7$ mol mol$^{-1}$. This is the result of the enhancement of the alcohol aggregation in detriment of the water hydrogen bonding network. Further, in this composition range, propan-2-ol and water show similar intra-diffusion coefficients, despite their difference in size and mass. Here, water molecules tend to be hydrogen bonded to the alcohol and are likely to propagate together with the alcohol cluster. Moreover, alcohol clusters are more stable than water clusters, i.e. one water molecule inside a methanol cluster diffuses out with more difficulty than from a water cluster[23].

As is the case for pure propan-2-ol, VACF of water and the alcohol in their mixture also display an unusually long tail, which becomes progressively important for increasing alcohol concentration. Again, the velocity persistence or long time memory of the system can be explained by steric hindrance effects. Relaxation time analyses[7,17] have shown that the relaxation time of water rapidly increases when propan-2-ol is added. For instance, the presence of two methyl groups in spatial proximity to the hydroxyl group reduces the probability for water and other propan-2-ol molecules to find a suitable new hydrogen bond partner[17]. As a consequence, the time required for restructuring the hydrogen bond network increases. Since diffusion involves a molecule changing its molecular neighborhood in solution, the hydroxyl group has to find an appropriate neighbor for

a new local equilibrium configuration. This so-called wait and switch mechanism[99] has also been found in other aqueous alcoholic mixtures by dielectric spectroscopy[99–102].

## Shear Viscosity

The shear viscosity of liquids is influenced by the intermolecular interactions and molecular shape[9], i.e. the presence of strong molecular attraction and bulky molecular groups hinder flow and leads to high shear viscosity values. In case of the studied mixture, the minimum of the thermodynamic factor and the Fick diffusion coefficient, where the non-ideality of the mixture is the strongest, i.e. minimum of the excess volume and the thermodynamic factor, corresponds to a maximum of the shear viscosity as expected from the Stokes-Einstein relation, cf. Fig. 5 (b) and Fig. 5 (d).

In general, the predicted shear viscosity agrees qualitatively and quantitatively with experimental literature data, despite an underestimation in the alcohol-rich region. The shear viscosity maximum at $x_{\mathrm{IPA}} \simeq 0.3$ mol mol$^{-1}$ is predicted with an excellent accuracy as can be seen in Fig. 5 (d).

## Microstructure

### Radial Distribution Functions

To elucidate the influence of water on the extent of nonrandom mixing, RDF were sampled in the entire composition range. Fig. 6 shows the present simulation results for the RDF of the oxygen-hydrogen (O-H) and oxygen-oxygen (O-O) pair interactions. The results from the TIP4P/2005 force field for pure water are in good agreement with experimental data reported by Soper and Philips[103] as can be seen in Fig. 6 (a) and Fig. 6 (b). The first and second peaks of the $g_{\mathrm{O-H}}(r)$ are located at $\simeq 1.86$ Å and $\simeq 3.21$ Å and have magnitudes of 1.60 and 1.56, respectively. The radius of the first coordination shell of $g_{\mathrm{O-H}}(r)$ for pure water is located at $r_m^{\mathrm{O-H}} \simeq 2.48$ Å with a magnitude of $\sim 0.17$. According to experimental data and present simulation results, $g_{\mathrm{O-O}}(r)$ of pure water shows three clearly identified coordination shells, located at $\sim \{3.2, 5.6, 7.9\}$ Å with mag-

nitudes of $\sim \{0.75, 0.88, 0.98\}$, respectively. The first maximum of $g_{\mathrm{O-O}}(r)$ is located at $\sim 2.81$ Å and has a magnitude of 3.22. The magnitude of its second maximum decreases by 64% as compared to the magnitude of the first one and the magnitude of its third maximum further decreases by only 6%. Moreover, the first maximum of $g_{\mathrm{O-O}}(r)$ for water-water interactions increases when less water is present, whereas the maximum of the corresponding IPA-IPA interactions decreases when less alcohol is present. This indicates that propan-2-ol molecules bond less with themselves when the water concentration increases, while water molecules bond more with themselves when their concentration decreases. This behavior is common for associating species mixed with non-associating ones[104].

Simulation results for the RDF at different mixture compositions are presented in Fig. 6. It can be seen that the second maximum of $g_{\mathrm{O-H}}(r)$ of water-water interactions shown in panel (a) is much more pronounced with decreasing water content. The $g_{\mathrm{O-H}}(r)$ for the alcohol-alcohol pair shows a similar behavior, i.e. the second coordination shell increases with decreasing water content as can be seen in Fig. 6 (e). Further, the magnitude of the first and second peaks of the $g_{\mathrm{O-H}}(r)$ for pure propan-2-ol is smaller than that of the unlike interaction, indicating preferential hydrogen bonding of the alcohol hydroxyl group to water, cf. Fig. 6 (e).

The average number of hydrogen bonds $\langle n_{\mathrm{O-H}} \rangle$ was calculated in the entire composition range employing the definition of the average running number $k_{xy} = 4\pi\rho_y \int_0^{r_c} r^2 g_{x-y}(r) dr$. Therein, $x$ stands for the central interaction site surrounded by interaction sites of type $y$, $\rho_y$ is the bulk density of interaction sites of type $y$, $g_{x-y}(r)$ represents the RDF of the pair involved in the running average number calculation and $r_c$ is an arbitrary site-site distance, which is usually selected as the radius of the first coordination shell, i.e. the location of the first minimum of $g_{\mathrm{O-H}}(r)$. Present results for pure water yield an average of 3.5 hydrogen bonds per water molecule. Further, the average number of hydrogen bonds per water molecule, corresponding to the water-water pair interactions in the binary mixture $\langle n_{\mathrm{O-H}} \rangle_{\mathrm{ww}}$ is given by

$$\frac{\langle n_{\mathrm{O-H}} \rangle_{\mathrm{ww}}}{8\pi x_{\mathrm{w}} \rho} \simeq \int_0^{r_m^{\mathrm{O-H}}} r^2 g_{\mathrm{O-H}}(r) dr + \int_0^{r_m^{\mathrm{H-O}}} r^2 g_{\mathrm{H-O}}(r) dr. \tag{11}$$

Subscript ww on the left side of Eq. (11) refers to hydrogen bonds formed when water molecules surround water molecules centered at the origin and $\rho$ is the bulk density of the mixture. Oxygen and hydrogen sites in the RDF belong to water molecules and $r_m^{\mathrm{O-H}}$ and $r_m^{\mathrm{H-O}}$ stand for the radius of their first minimum. Present results suggest that the radius of the first coordination shell slightly shifts towards shorter distances with increasing water content.

The average number of hydrogen bonds formed by the interactions between propan-2-ol molecules $\langle n_{\mathrm{O-H}}\rangle_{\mathrm{AA}}$, i.e. taking only alcohol molecules surrounding a central alcohol molecule into account, can be calculated from a modified version of Eq. (10), which can be obtained by replacing the total density with the partial density $x_{\mathrm{IPA}}\rho$ and the RDF of alcohol-alcohol interactions obtained from simulations of the binary mixture. Here, the radius of the first coordination shell shifts from 1.9 Å to 2.6 Å when the propan-2-ol mole fraction increases from 0.02 to 0.95 mol mol$^{-1}$. However, this microscopic feature yields its highest value at $x_{\mathrm{IPA}}$ = 0.1 mol mol$^{-1}$ and remains approximately constant for the remaining composition range.

The number of unlike hydrogen bonds, taking 2-propan-ol as central molecule $\langle n_{\mathrm{O-H}}\rangle_{\mathrm{Aw}}$, can be calculated from the RDF of the oxygen and hydrogen sites that belong to the unlike alcohol-water interaction. Similarly to Eq. (11), the number of unlike hydrogen bonds per 2-propanol molecule is

$$\frac{\langle n_{\mathrm{O-H}}\rangle_{\mathrm{Aw}}}{4\pi x_{\mathrm{IPA}}\rho} \simeq 2\int_0^{r_m^{\mathrm{O-H_w}}} r^2 g_{\mathrm{O-H_w}}(r)dr + \int_0^{r_m^{\mathrm{H-O_w}}} r^2 g_{\mathrm{H-O_w}}(r)dr, \tag{12}$$

where subscript w refers to the sites that belong to water molecules. The number of hydrogen bonds per propan-2-ol molecule calculated from present simulation values is in very good agreement with the literature values determined by X-ray scattering data analysis[16], a graphical comparison is shown in the supplementary information.

## Hydrogen Bonding

The behavior of the thermodynamic properties of aqueous alcoholic mixtures is governed by the hydrogen bond network. Thus, the presence of clusters due to bridging through hydrogen bonding

was analyzed. Fig. 7 shows the fraction of water and propan-2-ol molecules that are involved in hydrogen bonds with 1, 2, 3 or 4 neighbors as a function of composition. As expected, water and propan-2-ol molecules are rarely found as monomers in solution. Further, less than 3% of water molecules are hydrogen bonded to only one partner, cf. Fig. 7 (a). In case of propan-2-ol, the amount of dimers is somewhat higher, i.e. a maximum is reached at $x_{\mathrm{IPA}} = 0.25$ mol mol$^{-1}$ where around 9% of the alcohol molecules are hydrogen bonded with one water molecule. The amount IPA-IPA hydrogen bonded dimers increases with propan-2-ol mole fraction to reach 15% for the pure alcohol, cf. Fig. 7 (a). A similar behavior was observed for the fraction of water molecules that are hydrogen bonded with two propan-2-ol molecules, cf. Fig. 7 (b). The amount of water molecules involved in hydrogen bonding with another water molecule and one propan-2-ol molecule reaches a maximum of 7% at $x_{\mathrm{IPA}} \simeq 0.7$ mol mol$^{-1}$. As for propan-2-ol, around 40% of propan-2-ol molecules are hydrogen bonded to two water molecules at $x_{\mathrm{IPA}} = 0.1$ mol mol$^{-1}$ It should be noted that this mole fraction corresponds to the calculated minimum of the excess enthalpy. At $x_{\mathrm{IPA}} = 0.6$ mol mol$^{-1}$, approximately 30% of the propan-2-ol molecules are hydrogen bonded to one alcohol and one water molecule, cf. Fig. 7 (b).

As discussed above for the pure alcohol, 75% of the propan-2-ol molecules are hydrogen bonded to two alcohol molecules. Upon addition of water, the amount of such trimers reduces rapidly, e.g. when the water mole fraction has reached $x_{\mathrm{w}} = 0.1$ mol mol$^{-1}$, only 50% of the alcohol molecules are hydrogen bonded in this form, cf. Fig. 7 (b). The amount of propan-2-ol molecules involved in hydrogen bonding with three alcohol molecules is rather low. Nonetheless, in the water-rich region, i.e. $x_{\mathrm{IPA}} < 0.2$ mol mol$^{-1}$, a relatively large amount (up to 50%) of the propan-2-ol molecules are hydrogen bonded to three water molecules, cf. Fig. 7 (c). The distribution of hydrogen bonded tetramers with water as the central molecule with three alcohol molecules shows a similar behavior in the water-poor region. Further, a maximum of about 20% of the water molecules hydrogen bonded to one other water and two alcohol molecules was observed at $x_{\mathrm{IPA}} = 0.8$ mol mol$^{-1}$. At equimolar composition, a maximum of about 16% of the water molecules are hydrogen bonded to one alcohol and two water molecules, cf. Fig. 7 (c).

In pure water, most molecules are forming tetrahedral hydrogen bonded pentamers. Upon addition of propan-2-ol, the amount of water molecules in such pentamers is reduced gradually from more than 50% for pure water to less than 2% for $x_{\mathrm{IPA}}$ = 0.7 mol mol$^{-1}$. On the other hand, the amount of pentamers involving four propan-2-ol molecules increases to reach 25% in the alcohol-rich region, cf. Fig. 7 (d). The presence of two maxima, one of about 20% in the amount of water molecules hydrogen bonded to one alcohol and three water molecules at $x_{\mathrm{IPA}}$ = 0.3 mol mol$^{-1}$ and another one of 15% at $x_{\mathrm{IPA}}$ = 0.8 mol mol$^{-1}$, is noteworthy. Note that the minimum of the Fick diffusion coefficient and the shear viscosity maximum is also located at $x_{\mathrm{IPA}} \simeq 0.3$ mol mol$^{-1}$.

Based on this hydrogen bonding statistics, it is also possible to calculate the average number of hydrogen bonds per water or alcohol molecule. Fig. 8 shows the results for the total number of hydrogen bonds differentiating between the involved species, i.e. water-water (w-w), propan-2-ol-water (w-IPA) and propan-2-ol-propan-2-ol (IPA-IPA). It can be seen that the total amount of hydrogen bonds per propan-2-ol molecule increases when water is added, resulting in a stabilization of alcohol molecules. Note that the average number hydrogen bonds with other alcohol molecules decreases, while the number of hydrogen bonds with water increases. Thus, water molecules displace alcohol molecules as hydrogen bonding partners of propan-2-ol, causing a rearrangement of the local hydrogen bonding structure[23]. In case of water, the average number of hydrogen bonds decreases in the mixture. Upon addition of propan-2-ol, the tetrahedral structure of water is gradually disrupted by dominating alcohol molecules[7]. At $x_{\mathrm{IPA}} \simeq 0.6$ to 0.7 mol mol$^{-1}$, the average number of unlike hydrogen bonds between water and propan-2-ol is higher than that between the individual species, i.e. IPA-IPA and w-w, respectively. Note that the maximum of the excess enthalpy is located near these compositions.

In their classical paper Dixit et al.[105] introduced the concept of excess hydrogen bonding to quantify the amount of hydrogen bonds created or destroyed upon mixing. Fig. 9 shows the calculated excess hydrogen bonds as a function of composition. It can be seen that there is an impressive similarity with the composition behavior of the excess enthalpy where a maximum and a minimum

are present, cf. Fig. 4. In fact, the positive excess enthalpy of the propan-2-ol + water mixture has been attributed to steric hindrance effects which impede ideal hydrogen bond formation[106]. This demonstrates a clear relationship between excess enthalpy and excess hydrogen bonding. Furthermore, the transition region from the net increase to the net decrease of hydrogen bonding, i.e. a change in the slope of the curve, occurs in the region where the minimum of the Fick diffusion coefficient $x_{\mathrm{IPA}}$ = 0.3 mol mol$^{-1}$ is found.

### Snapshots Analysis

In general, snapshots represent only one micro-state of a molecular system. However, in the case of micro-heterogeneous mixtures with associating components, a single micro-state may well represent all possible micro-states, being permutations of the segregation patterns[104]. Fig. 10 shows snapshots of simulation volumes for four different compositions $x_{\mathrm{IPA}}$ = 0.1, 0.3, 0.5 and 0.9 mol mol$^{-1}$. Moreover, the spatial configuration of selected clusters are also shown. In case of low alcohol content, propan-2-ol molecules tend to occupy cavities inside the water hydrogen bonding structure, the alcohol hydroxyl groups are rather hydrogen bonded to water than to other propan-2-ol molecules. At $x_{\mathrm{IPA}}$ = 0.3 and 0.5 mol mol$^{-1}$, it can be seen that water and propan-2-ol form segregated domains. This observation corresponds to low values of the thermodynamic factor and Fick diffusion coefficient. The tendency of water molecules to aggregate with propan-2-ol molecules can be clearly seen in the snapshots for the lowest water mole fraction $x_{\mathrm{IPA}}$ = 0.9 mol mol$^{-1}$.

## Conclusion

The microstructure of liquid water + propan-2-ol was analyzed by means of molecular simulation techniques. Despite of the highly non-ideality of this aqueous mixture, it was demonstrated that the employed force field combination is able to accurately predict excess properties and transport coefficients at 298.15 K and 0.1 MPa in the entire concentration range.

It was found that the VACF that constitute the self- and intra-diffusion coefficients of propan-2-ol have an unusually long time memory because of steric hindrance effects. Similar values of the intra-diffusion coefficients of water and propan-2-ol in the alcohol rich composition range are a consequence of stable alcohol-water clusters. Further, it was observed that the minimum of the Fick diffusion coefficient and the shear viscosity maximum correspond to the minimum of the thermodynamic factor at $x_{\mathrm{IPA}} = 0.3$ mol mol$^{-1}$. Here, the strongest microscopic inhomogeneities were noticed in simulation volumes snapshots.

Radial distribution functions and hydrogen bonding statistics suggest that pure propan-2-ol is on average involved in two hydrogen bonds. Upon addition of water, the total amount of hydrogen bonds per propan-2-ol molecule increases because water molecules displace alcohol molecules as hydrogen bonding partners of propan-2-ol and the local hydrogen bonding structure is rearranged. Moreover, the radius of the first coordination shell of propan-2-ol becomes slightly smaller with increasing water content, resulting in a stabilization of alcohol molecules. On the other hand, present results showed that the total average amount of hydrogen bonds per water molecule decreases upon its dilution from approximately 3.6 to 3.0.

One of the most revealing insights is given by the similarity found between the excess number of hydrogen bonds and the excess enthalpy, where a maximum and a minimum are present, implying a strong correlation between these properties. Further, the minimum of the Fick diffusion coefficient is located in the region where the transition from a net increase to a net decrease of hydrogen bonding occurs.

# Acknowledgement

This work was funded by the Deutsche Forschungsgemeinschaft (DFG) under the grant VR 6/11-1. The simulations were carried out on the national supercomputer Hazel hen at the High Performance Computing Center Stuttgart (HLRS) within the project MMHBF2. The presented research was conducted under the auspices of the Boltzmann-Zuse Society of Computational Molecular

Engineering (BZS). The authors warmheartedly thank Elmar Baumhögger for his TOC artwork.

## Supplementary Information

Methodology for excess properties; molecular simulation details; workflow of the present force field parameterization process; comparison with other force fields; velocity autocorrelation function of propan-2-ol; initial decay of the velocity autocorrelation function of propan-2-ol; number of hydrogen bonds per oxygen atom as a function of the propan-2-ol mole fraction; tables with simulation results.

## References

(1) Dougan, L.; Hargreaves, R.; Bates, S. P.; Finney, J. L.; Réat, V.; Soper, A. K.; Crain, J. Segregation in Aqueous Methanol Enhanced by Cooling and Compression. *J. Chem. Phys.* **2005**, *122*, 174514–174520.

(2) Corsaro, C.; Spooren, J.; Branca, C.; Leone, N.; Broccio, M.; Kim, C.; Chen, S.-H.; Stanley, H. E.; Mallamace, F. Clustering Dynamics in Water/Methanol Mixtures: A Nuclear Magnetic Resonance Study at 205 K $<$ T $<$ 295 K. *J. Phys. Chem. B* **2008**, *112*, 10449–10454.

(3) Ono, T.; Horikawa, K.; Ota, M.; Sato, Y.; Inomata, H. Insight into the Local Composition of the Wilson Equation at High Temperatures and Pressures through Molecular Simulations of Methanol–Water Mixtures. *J. Chem. Eng. Data* **2014**, *59*, 1024–1030.

(4) Frank, H. S.; Evans, M. W. Free Volume and Entropy in Condensed Systems III. Entropy in Binary Liquid Mixtures; Partial Molal Entropy in Dilute Solutions; Structure and Thermodynamics in Aqueous Electrolytes. *J. Chem. Phys.* **1945**, *13*, 507–532.

(5) Li, R.; D'Agostino, C.; McGregor, J.; Mantle, M. D.; Zeitler, J. A.; Gladden, L. F. Mesoscopic Structuring and Dynamics of Alcohol/Water Solutions Probed by Terahertz Time-Domain Spectroscopy and Pulsed Field Gradient Nuclear Magnetic Resonance. *J. Phys. Chem. B* **2014**, *118*, 10156–10166.

(6) Tomza, P.; Czarnecki, M. A. Microheterogeneity in Binary Mixtures of Propyl Alcohols with Water: NIR Spectroscopic, Two-Dimensional Correlation and Multivariate Curve Resolution Study. *J. Mol. Liq.* **2015**, *209*, 115–120.

(7) McGregor, J.; Li, R.; Zeitler, J. A.; D'Agostino, C.; Collins, J. H. P.; Mantle, M. D.; Manyar, H.; Holbrey, J. D.; Falkowska, M.; Youngs, T. G. A. et al. Structure and Dynamics of Aqueous 2-Propanol: A THz-TDS, NMR and Neutron Diffraction Study. *Phys. Chem. Chem. Phys.* **2015**, *17*, 30481–30491.

(8) Wrzeszcz, W.; , P.; Kwaśniewicz, M.; Mazurek, S.; Szostak, R.; Czarnecki, M. A. Microheterogeneity in Binary Mixtures of Methanol with Aliphatic Alcohols: ATR-IR/NIR Spectroscopic, Chemometrics and DFT Studies. *RSC Adv.* **2016**, *6*, 37195–37202.

(9) Jora, M. Z.; Cardoso, M. V. C.; Sabadini, E. Correlation between Viscosity, Diffusion Coefficient and Spin-Spin Relaxation Rate in 1H NMR of Water-Alcohols Solutions. *J. Mol. Liq.* **2017**, *238*, 341–346.

(10) Raschke, T. M.; Levitt, M. Nonpolar Solutes Enhance Water Structure within Hydration Shells While Reducing Interactions between Them. *PNAS* **2005**, *102*, 6777–6782.

(11) Babic, D.; Pfennig, A. Comparison of Two Modeling Approaches for Describing Intra-Diffusion in Liquid Lennard–Jones Mixtures Containing a Self-Associating Component. *Fluid Phase Equilib.* **2006**, *245*, 140–148.

(12) Kamath, G.; Georgiev, G.; Potoff, J. J. Molecular Modeling of Phase Behavior and Microstructure of Acetone–Chloroform–Methanol Binary Mixtures. *J. Phys. Chem. B* **2005**, *109*, 19463–19473.

(13) Gereben, O.; Pusztai, L. Investigation of the Structure of Ethanol– Water Mixtures by Molecular Dynamics Simulation I: Analyses Concerning the Hydrogen–Bonded Pairs. *J. Phys. Chem. B* **2015**, *119*, 370–384.

(14) , G.; Vrabec, J.; Hasse, H. Prediction of Self-Diffusion Coefficient and Shear Viscosity of Water and Its Binary Mixtures with Methanol and Ethanol by Molecular Simulation. *J. Chem. Phys.* **2011**, *134*, 074508.

(15) Bye, J. W.; Freeman, C. L.; Howard, J. D.; Herz, G.; McGregor, J.; Falconer, R. J. Analysis of Mesoscopic Structured 2-Propanol/Water Mixtures Using Pressure Perturbation Calorimetry and Molecular Dynamic Simulation. *J. Solution Chem.* **2017**, *46*, 175–189.

(16) Takamuku, T.; Saisho, K.; Aoki, S.; Yamaguchi, T. Large-Angle X-ray Scattering Investigation of the Structure of 2-Propanol–Water Mixtures . *Z. Naturforsch. A* **2002**, *57*, 982–994.

(17) Sato, T.; Buchner, R. The Cooperative Dynamics of the H-Bond System in 2-Propanol/Water Mixtures: Steric Hindrance Effects of Nonpolar Head Group. *J. Chem. Phys.* **2003**, *119*, 10789–10800.

(18) Soliman, K.; Marschall, E. Viscosity of Selected Binary, Ternary and Quaternary Liquid Mixtures. *J. Chem. Eng. Data* **1990**, *35*, 375–381.

(19) Fidler, J.; Rodger, P. M. Solvation Structure around Aqueous Alcohols. *J. Phys. Chem. B* **1999**, *103*, 7695–7703.

(20) Anisimov, V. M.; Vorobyvov, I. V.; Roux, B.; MacKerell, A. D. Polarizable Empirical Force Field for the Primary and Secondary Alcohol Series Based on the Classical Drude Model. *J. Chem. Theory Comput.* **2007**, *3*, 1927–1946.

(21) Cardona, J.; Sweatman, M. B.; Lue, L. Molecular Dynamics Investigation of the Influence of the Hydrogen Bond Networks in Ethanol/Water Mixtures on Dielectric Spectra. *J. Phys. Chem. B* **2018**, *122*, 1505–1515.

(22) Galicia-Andrés, E.; Dominguez, H.; Pusztai, L.; Pizio, O. Composition Dependence of Thermodynamic, Dynamic and Dielectric Properties of Water–Methanol Model Mixtures. Molecular Dynamics Simulation Results with the OPLS-AA Model for Methanol. *J. Mol. Liq.* **2015**, *212*, 70–78.

(23) Zhang, N.; Shen, Z.; Chen, C.; He, G.; Hao, C. Effect of Hydrogen Bonding on Self-Diffusion in Methanol/Water Liquid Mixtures: A Molecular Dynamics Simulation Study. *J. Mol. Liq.* **2015**, *203*, 90–97.

(24) Eckl, B.; Vrabec, J.; Hasse, H. Set of Molecular Models Based on Quantum Mechanical Ab Initio Calculations and Thermodynamic Data. *J. Phys. Chem. B* **2008**, *112*, 12710–12721.

(25) Deublein, S.; Metzler, P.; Vrabec, J.; Hasse, H. Automated Development of Force Fields for the Calculation of Thermodynamic Properties: Acetonitrile as a Case Study. *Mol. Sim.* **2013**, *39*, 109–118.

(26) Muñoz-Muñoz, Y. M.; , G.; Llano-Restrepo, M.; Vrabec, J. Lennard-Jones Force Field Parameters for Cyclic Alkanes from Cyclopropane to Cyclohexane. *Fluid Phase Equilib.* **2015**, *404*, 150–160.

(27) Muñoz-Muñoz, Y. M.; Hsieh, C.-M.; Vrabec, J. Understanding the Differing Fluid Phase Behavior of Cyclohexane + Benzene and Their Hydroxylated or Aminated Forms. *J. Phys. Chem. B.* **2017**, *121*, 5374–5384.

(28) Abascal, J. L. F.; Vega, C. A General Purpose Model for the Condensed Phases of Water: TIP4P/2005. *J. Chem. Phys.* **2005**, *123*, 234505.

(29) Yu, Y. X.; Gao, G. H. Study on Self-Diffusion in Water, Alcohols and Hydrogen Fluoride by the Statistical Associating Fluid Theory. *Fluid Phase Equilib.* **2001**, *179*, 165–179.

(30) Stillinger, F. H. Water Revisited. *Science* **1980**, *209*, 451–457.

(31) Haughney, M.; Ferrario, M.; McDonald, I. R. Molecular-Dynamics Simulation of Liquid Methanol. *J. Phys. Chem.* **1987**, *91*, 4934–4940.

(32) Henchman, R. H.; Irudayam, S. J. Topological Hydrogen-Bond Definition to Characterize the Structure and Dynamics of Liquid Water. *J. Phys. Chem. B* **2010**, *114*, 16792–16810.

(33) Rutkai, G.; Köster, A.; Guevara-Carrion, G.; Janzen, T.; Schappals, M.; Glass, C. W.; Bernreuther, M.; Wafai, A.; Stephan, S.; Kohns, M. et al. ms2: A Molecular Simulation Tool for Thermodynamic Properties, Release 3.0. *Comp. Phys. Commun.* **2017**, *221*, 343–351.

(34) Green, M. S. Markoff Random Processes and the Statistical Mechanics of Time-Dependent Phenomena. II. Irreversible Processes in Fluids. *J. Chem. Phys.* **1954**, *22*, 398–414.

(35) Kubo, R. Statistical-Mechanical Theory of Irreversible Processes I. General Theory and Simple Applications to Magnetic and Conduction Problems. *J. Phys. Soc. Jpn.* **1957**, *12*, 570–586.

(36) Taylor, R.; Krishna, R. *Multicomponent Mass Transfer*; John Wiley & Sons: New York, 1993.

(37) Krishna, R.; Wesselingh, J. A. The Maxwell-Stefan Approach to Mass Transfer. *Chem. Eng. Sci.* **1997**, *52*, 861–911.

(38) Poling, B. E.; Prausnitz, J. M.; O'Connell, J. P. *The Properties of Gases and Liquids*, 5th ed.; McGraw-Hill: New York, 2001.

(39) Wilson, G. M. Vapor-Liquid Equilibrium. A New Expression for the Excess Free Energy of Mixing. *J. Am. Chem. Soc.* **1964**, *86*, 127–130.

(40) Sazonov, V. P. Liquid-Liquid-Vapor Isothermal Equilibrium in a Nitromethane-Isopropyl Alcohol-Water System. *Zh. Prikl. Khim.* **1986**, *59*, 1451–1456.

(41) Taylor, R.; Kooijman, H. A. Composition Derivatives of Activity Coefficient Models (for the Estimation of Thermodynamic Factors in Diffusion). *Chem. Eng. Commun.* **1991**, *102*, 87–106.

(42) Alfe, D.; Gillan, M. J. First-Principles Calculation of Transport Coefficients . *Phys. Rev. Lett.* **1988**, *81*, 5161–5164.

(43) Yeh, I. C.; Hummer, G. System-Size Dependence of Diffusion Coefficients and Viscosities from Molecular Dynamics Simulations with Periodic Boundary Conditions. *J. Phys. Chem. B* **2004**, *108*, 15873–15879.

(44) Jamali, S. H.; Wolff, L.; Becker, T. M.; Bardow, A.; Vlugt, T. J. H.; Moultos, O. A. Finite-Size Effects of Binary Mutual Diffusion Coefficients from Molecular Dynamics. *J. Chem. Theory Comput.* **2018**, *14*, 2667–2677.

(45) Daivis, P. J.; Evans, D. J. Transport Coefficients of Liquid Butane Near the Boiling Point by Equilibrium Molecular Dynamics. *J. Chem. Phys.* **1995**, *103*, 4261–4265.

(46) Gereben, O.; Pusztai, L. System Size and Trajectory Length Dependence of the Static Structure Factor and the Diffusion Coefficient as Calculated from Molecular Dynamics Simulations: The Case of SPC/E Water. *J. Mol. Liq.* **2011**, *161*, 36–40.

(47) Zhang, Y.; Otani, Y.; Maginn, E. J. Reliable Viscosity Calculation from Equilibrium Molecular Dynamics Simulations: A Time Decomposition Method. *J. Chem. Theory Comput.* **2015**, *11*, 3537–3546.

(48) NIST Computational Chemistry Comparison and Benchmark Database. `http://cccbdb.nist.gov`, (Accessed: 2018-08-20).

(49) Essén, H.; Svenddon, M. Calculation of Coordinates from Molecular Geometric Parameters and the Concept of a Geometric Calculator. *Comput. Chem.* **1996**, *20*, 4002–4006.

(50) Hales, J.; Ellender, J. Liquid Densities from 293 to 490 K of Nine Aliphatic Alcohols. *J. Chem. Thermodyn.* **1976**, *8*, 1177–1184.

(51) Smith, B.; Srivastava, R. *Thermodynamic Data for Pure Compounds. Part B. Halogenated Hydrocarbons and Alcohols*; Elsevier: Amsterdam, 1986.

(52) Fox, O.; Morcillo, J.; Mendez, A. Compressibilities of the Vapors of Several Alcohols. *An. R. Soc. Esp. Quím.* **1954**, *17B*.

(53) Kretschmer, C. B.; Wiebe, R. Pressure-Volume-Temperature Relationships of Alcohol Vapors2. *J. Am. Chem. Soc.* **1954**, *76*, 2579–2583.

(54) *TRC Thermodynamic Tables-Non-Hydrocarbons*; The Texas A&M University System: College Station TX, 1998.

(55) Timmermans, J. *Physico-Chemical Constants of Pure Organic Substances; Vol II*; Elsevier: New York, 1965.

(56) Ullmann, F.; Gerhartz, W.; Yamamoto, Y. S. *Ullmann's Encyclopedia of Industrial Chemistry 5th Ed.*; VCH Publishers: Deerfield Beach, FL, 1985.

(57) Rowley, R. L.; Wilding, W. V.; Oscarson, J. L.; Yang, Y.; Giles, N. F. *DIPPR: Data Compilation of Pure Chemical Properties*; Design Institute for Physical Properties, AIChE: New York, 2010.

(58) Van Leeuwen, M. E. Prediction of the Vapour-Liquid Coexistence Curve of Alkanols by Molecular Simulation. *Molecular Physics* **1996**, *87*, 87–101.

(59) Chen, B.; Potoff, J. J.; Siepmann, J. I. Monte Carlo Calculations for Alcohols and Their Mixtures with Alkanes. Transferable Potentials for Phase Equilibria. 5. United-Atom Description of Primary, Secondary, and Tertiary Alcohols. *The Journal of Physical Chemistry B* **2001**, *105*, 3093–3104.

(60) Xin, N.; Liu, Y.; Guo, X.; Liu, X.; Zhang, Y.; He, M. Determination of Critical Properties for Binary and Ternary Mixtures Containing Propanol and Alkanes Using a Flow View-Type Apparatus. *J. Supercrit. Fluids* **2016**, *108*, 35–44.

(61) Gude, M.; Teja, A. S. Vapor-Liquid Critical Properties of Elements and Compounds. 4. Aliphatic Alkanols. *J. Chem. Eng. Data* **1995**, *40*, 1025–1036.

(62) Stone, A. J. *The Theory of Intermolecular Forces*; Clarendon Press: Oxford, 1996.

(63) Pang, F.-M.; Seng, C.-E.; Teng, T.-T.; Ibrahim, M. Densities and Viscosities of Aqueous Solutions of 1-Propanol and 2-Propanol at Temperatures from 293.15 K to 333.15 K. *J. Mol. Liq.* **2007**, *136*, 71–78.

(64) Yang, C.; Lai, H.; Liu, Z.; Ma, P. Densities and Viscosities of Diethyl Carbonate + Toluene, + Methanol, and + 2-Propanol from (293.15 to 363.15) K. *J. Chem. Eng. Data* **2006**, *51*, 584–589.

(65) Ku, H. C.; Tu, C. H. Density and Viscosity of Binary Mixtures of Propan-2-ol, 1-Chlorobutane, and Acetonitrile. *J. Chem. Eng. Data* **1998**, *43*, 465–468.

(66) Moha-Ouchane, M.; Boned, C.; Allal, A.; Benseddik, M. Viscosity and Excess Volume at High Pressures in Associative Binaries. *Int. J. Thermophys.* **1998**, *19*, 161–189.

(67) Partington, J. R.; Hudson, R. F.; Bagnall, K. W. Self-diffusion of Aliphatic Alcohols. *Nature* **1952**, *169*, 583–584.

(68) Pratt, K. C.; Wakeham, W. A. Self-diffusion in Water and Monohydric Alcohols. *J. Chem. Soc., Faraday Trans. 2* **1977**, *73*, 997–1002.

(69) Taniewska-Osinska, S.; Kacperska, A. Viscosity Measurements of NaI Solutions in Water-Isopropanol Mixtures at Several Temperatures Viscosity Measurements of NaI Solutions in Water-Isopropanol Mixtures at Several Temperatures. *Folia Chim. Univ. Lodz.* **1983**, *2*, 25–31.

(70) Feng, H.; Gao, W.; Sun, Z.; Chen, L.; Lüdemann, H.-D.; Lei, B.; Li, G. The Self-Diffusion and Hydrogen Bond Interaction in Neat Liquid Alkanols: A Molecular Dynamic Simulation Study. *Molecular Simulation* **2014**, *40*, 1074–1084.

(71) Kulschewski, T.; Pleiss, J. A Molecular Dynamics Study of Liquid Aliphatic Alcohols: Simulation of Density and Self-Diffusion Coefficient Using a Modified OPLS Force Field. *Molecular Simulation* **2013**, *39*, 754–767.

(72) Alder, B. J.; Wainwright, T. E. Decay of the Velocity Autocorrelation Function. *Phys. Rev. A* **1970**, *1*, 18–21.

(73) Takamuku, T.; Saisho, K.; Nozawa, S.; Yamaguchi, T. X-Ray Diffraction Studies on Methanol–Water, Ethanol–Water, and 2-Propanol–Water Mixtures at Low Temperatures. *J. Mol. Liq.* **2005**, *119*, 133–146.

(74) Schnabel, T.; Srivastava, A.; Vrabec, J.; Hasse, H. Hydrogen Bonding of Methanol in Supercritical CO2: Comparison Between 1H-NMR Spectroscopic Data and Molecular Simulation Results. *J. Phys. Chem. B* **2007**, *111*, 9871–9878.

(75) Schnabel, T.; Vrabec, J.; Hasse, H. Henry's law Constants of Methane, Nitrogen, Oxigen and Carbon dioxide in Ethanol from 273 to 498 K: Prediction from Molecular Simulation. *Fluid Phase Equilib.* **2005**, *233*, 134–143.

(76) Sakurai, M. Partial Molar Volumes in Aqueous Mixtures of Nonelectrolytes. II. Isopropyl Alcohol. *J. Solution Chem.* **1988**, *17*, 267–275.

(77) Herráez, J. V.; Belda, R. Refractive Indices, Densities and Excess Molar Volumes of Monoalcohols + Water. *J. Solution Chem.* **2006**, *35*, 1315–1328.

(78) Navarro, P.; Larriba, M.; Garcia, S.; Garcia, J.; Rodriguez, F. Properties of Binary and Ternary Mixtures of 2-Propanol, Water, and 1-Butyl-3-methylimidazolium Tetrafluoroborate Ionic Liquid. *J. Chem. Eng. Data* **2012**, *57*, 1165–1173.

(79) Lama, R. F.; Lu, B. C.-Y. Excess Thermodynamic Properties of Aqueous Alcohol Solutions. *J. Chem. Eng. Data* **1965**, *10*, 216–219.

(80) Denda, M.; Touhara, H.; Nakanishi, K. Excess Molar Enthalpies for (Water + a Fluoroalkanol). *J. Chem. Thermodyn.* **1987**, *19*, 539–542.

(81) Battler, J. R.; Clark, W. M.; Rowley, R. L. Excess Enthalpy and Liquid-Liquid Equilibrium Surfaces for the Cyclohexane-2-Propanol-Water System from 293.15 to 323.15 K. *J. Chem. Eng. Data* **1985**, *30*, 254–259.

(82) Marongiu, B.; Ferino, I.; Monaci, R.; Solinas, V.; Torrazza, S. Thermodynamic Properties of Aqueous Non-Electrolyte Mixtures. Alkanols + Water Systems. *J. Mol. Liq.* **1984**, *28*, 228–247.

(83) Davis, M. I.; Rubio, J. B.; Douheret, G. Excess Molar Enthalpies of 2-Propanol + Water at 25 °C. *Thermochim. Acta* **1995**, *259*, 177–185.

(84) González-Salgado, D.; Nezbeda, I. Excess Properties of Aqueous Mixtures of Methanol: Simulation Versus Experiment. *Fluid Phase Equilib.* **2006**, *240*, 161–166.

(85) Weerasinghe, S.; Smith, P. E. A Kirkwood–Buff Derived Force Field for Methanol and Aqueous Methanol Solutions. *J. Phys. Chem. B* **2005**, *109*, 15080–15086.

(86) Gomide Freitas, L. C. Monte Carlo Simulation of the Binary Liquid Mixture Water–Methanol. *J. Mol. Struct.* **1993**, *282*, 151–158.

(87) Yu, H.; Geerke, D. P.; Liu, H.; van Gunsteren, W. F. Molecular Dynamics Simulations of Liquid Methanol and Methanol–Water Mixtures with Polarizable Models. *J. Comput. Chem.* **2006**, *27*, 1494–1504.

(88) Zhong, Y.; Warren, G. L.; Patel, S. Thermodynamic and Structural Properties of Methanol-Water Solutions Using Nonadditive Interaction Models. *J. Comput. Chem.* **2008**, *29*, 1142–1152.

(89) Guevara-Carrion, G.; Janzen, T.; Muñoz-Muñoz, Y. M.; Vrabec, J. Mutual Diffusion of Binary Liquid Mixtures Containing Methanol, Ethanol, Acetone, Benzene, Cyclohexane, Toluene, and Carbon Tetrachloride. *J. Chem. Phys.* **2016**, *144*, 124501.

(90) Van Ness, H. C.; Byer, S. M.; Gibbs, R. E. Vapor-Liquid Equilibrium: Part I. An Appraisal of Data Reduction Methods. *AIChE J.* **1978**, *19*, 238–244.

(91) Fredenslund, A.; Gmehling, J.; Rasmussen, P. *Vapor-Liquid Equilibria Using UNIFAC, A Group Contribution Method*; Elsevier: Amsterdam, 1977.

(92) Herington, E. F. G. A Thermodynamic Test for the Internal Consistency of Experimental Data on Volatility Ratios. *Nature* **1947**, *160*, 610–611.

(93) Redlich, O.; Kister, A. T. Algebraic Representation of Thermodynamic Properties and the Classification of Solutions. *Ind. Eng. Chem.* **1948**, *40*, 345–348.

(94) Leaist, D. G.; Deng, Z. Doubling of the Apparent Rates of Diffusion of Aqueous Propanols near Compositions of Maximum Refractive Index. *J. Phys. Chem.* **1992**, *96*, 2016–2018.

(95) Pratt, K. C.; Wakeham, W. A. The Mutual Diffusion Coefficient for Binary Mixtures of Water and the Isomers of Propanol. *Proc. R. Soc. London* **1975**, *A342*, 186–203.

(96) Mialdun, A.; Yasnou, V.; Shetsova, V.; Königer, A.; Köhler, W.; Alonso de Mezquia, D.; Bou-Ali, M. M. A Comprehensive Study of Diffusion, Thermodiffusion, and Soret Coefficients of Water- Isopropanol Mixtures. *J. Chem. Phys.* **2012**, *136*, 244512.

(97) Krishna, R. Uphill Diffusion in Multicomponent Mixtures. *Chem. Soc. Rev.* **2015**, *44*, 2812–2836.

(98) Zhang, N.; Li, W.; Chen, C.; Zuo, J.; Weng, L. Molecular Dynamics Study on Water Self-Diffusion in Aqueous Mixtures of Methanol, Ethylene Glycol and Glycerol: Investigations from the Point of View of Hydrogen Bonding. *Mol. Phys.* **2013**, *111*, 939–949.

(99) Petong, P.; Pottel, R.; Kaatze, U. Dielectric Relaxation of H-Bonded Liquids. Mixtures of Ethanol and n-Hexanol at Different Compositions and Temperatures. *J. Phys. Chem. A* **1999**, *103*, 6114–6121.

(100) Petong, P.; Pottel, R.; Kaatze, U. Water-Ethanol Mixtures at Different Compositions and Temperatures. A Dielectric Relaxation Study. *J. Phys. Chem. A* **2000**, *104*, 7420–7428.

(101) Sato, T.; Buchner, R. Dielectric Relaxation Processes in Ethanol/Water Mixtures. *J. Phys. Chem. A* **2004**, *108*, 5007–5015.

(102) Sato, T.; Buchner, R. Cooperative and Molecular Dynamics of Alcohol/Water Mixtures: The View of Dielectric Spectroscopy. *J. Mol. Liq.* **2005**, *117*, 23–31.

(103) Soper, A.; Phillips, M. A New Determination of the Structure of Water at 25°C. *Chem. Phys.* **1986**, *107*, 47–60.

(104) Požar, M.; Lovrinčević, B.; Zoranić, L.; Primorać, T.; Sokolić, F.; Perera, A. Micro-Heterogeneity Versus Clustering in Binary Mixtures of Ethanol With Water or Alkanes. *Phys. Chem. Chem. Phys.* **2016**, *18*, 23971–23979.

(105) Dixit, S.; Crain, J.; Poon, W. C. K.; Finney, J. L.; Soper, A. K. Molecular Segregation Observed in a Concentrated Alcohol-Water Solution. *Nature* **2002**, *416*, 829–832.

(106) Lam, R. K.; Smith, J. W.; Saykally, R. J. Communication: Hydrogen Bonding Interactions in Water-Alcohol Mixtures from X-Ray Absorption Spectroscopy. *J. Chem. Phys.* **2016**, *144*, 191103.

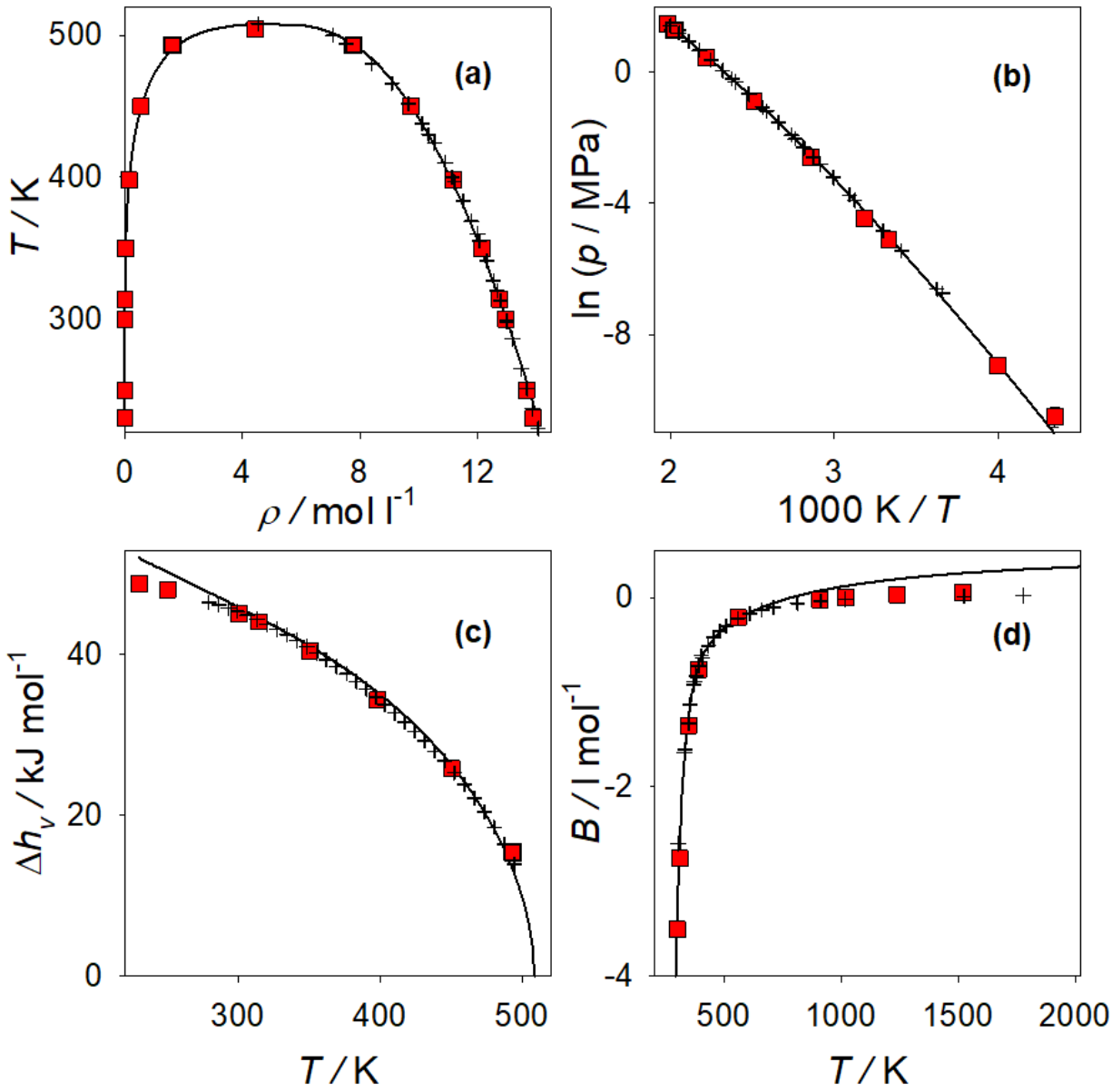


Figure 1: Saturated densities (a), vapor pressure (b), enthalpy of vaporization (c) and second virial coefficient (d) of propan-2-ol. Present molecular simulation results (red squares) are compared with experimental data (+) from the literature[50–56] and the DIPPR correlations[57] (–).

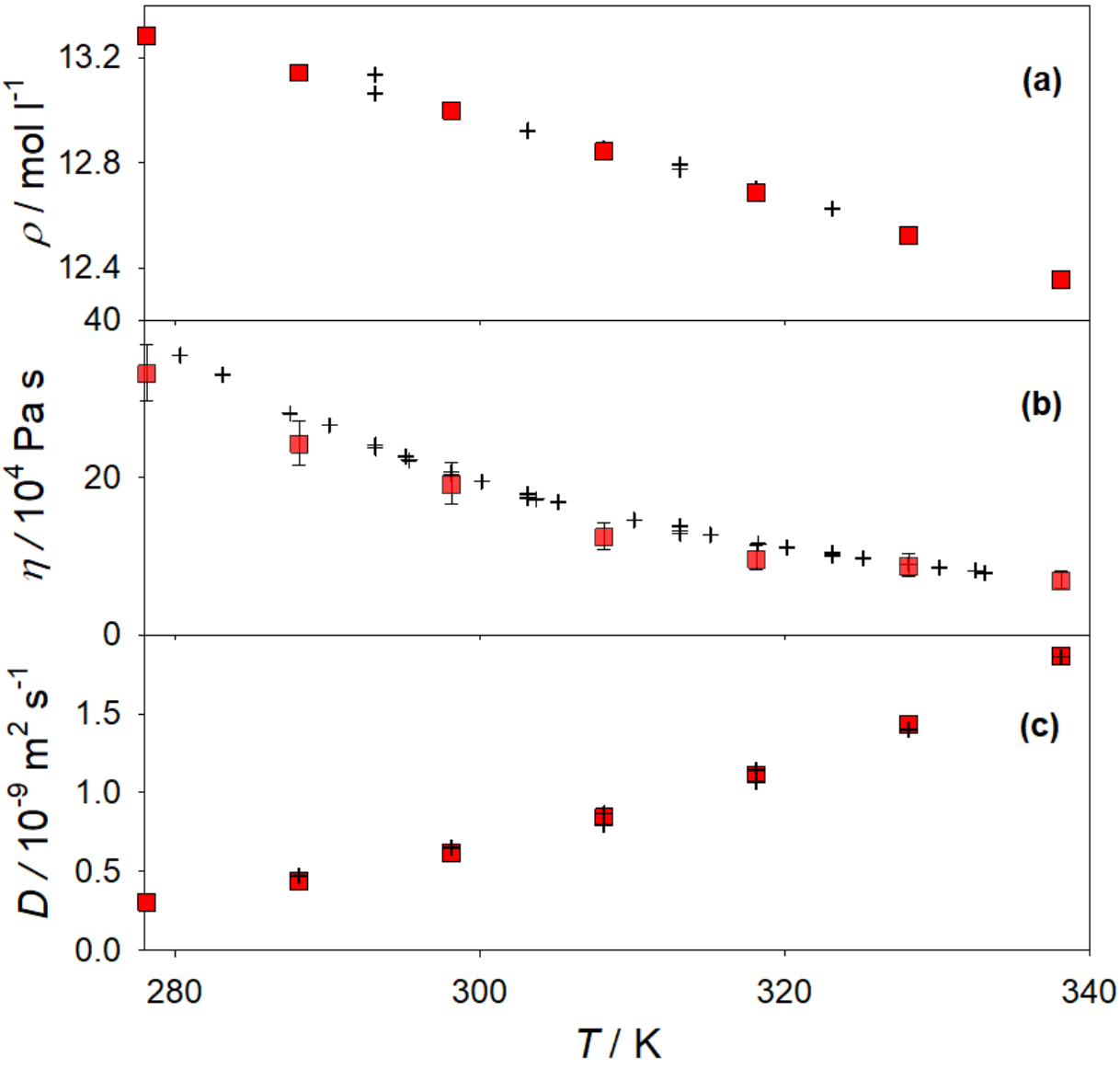


Figure 2: Density (a), shear viscosity (b) and self-diffusion coefficient (c) of liquid propan-2-ol at 0.1 MPa. Present molecular simulation results (red squares) are compared with experimental data (+) from the literature[63–69].

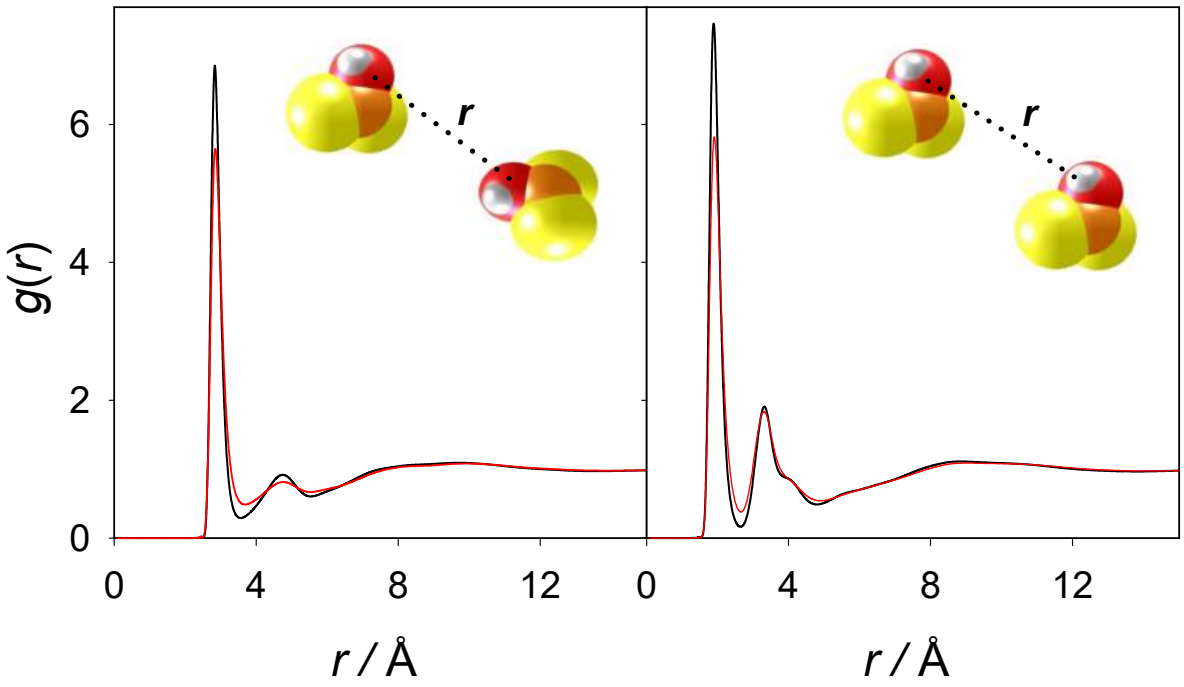


Figure 3: Oxygen-oxygen (left) and oxygen-hydrogen (right) radial distribution functions of propan-2-ol at 278.15 K (black lines) and 338.15 K (red lines). White, red, orange and yellow sites represent hydrogen and oxygen atoms, methanetriyl (CH) and methyl ($CH_3$) sites of the present force field.

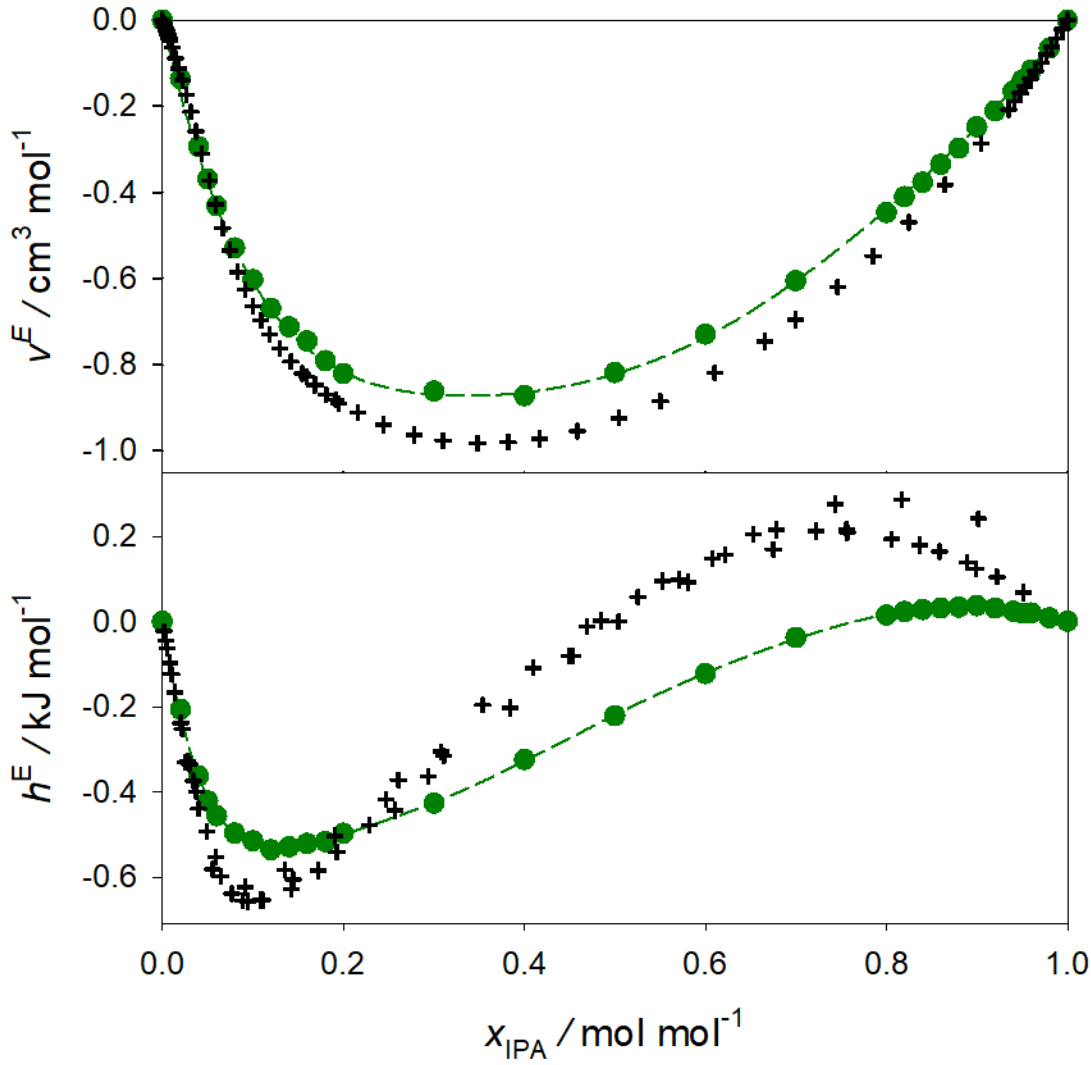


Figure 4: Excess volume (top) and excess enthalpy (bottom) of propan-2-ol + water at 298.15 K and 0.1 MPa. Simulation results (green symbols) are compared with experimental data (+) from the literature[63,76–83]. The dashed line represents the Redlich-Kister correlation that serves as a guide to the eye

.

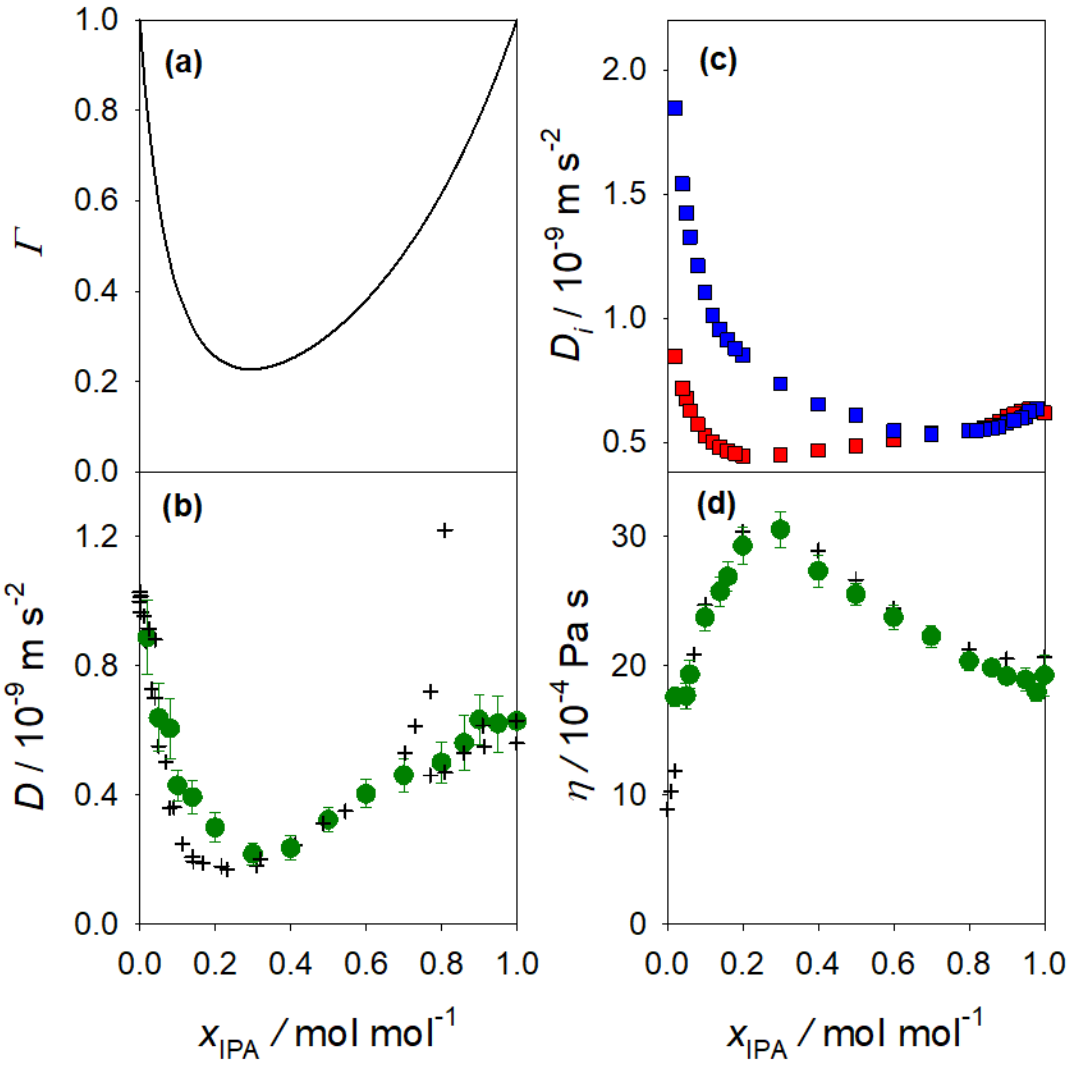


Figure 5: Properties of propan-2-ol + water at 298.15 K and 0.1 MPa. (a) Thermodynamic factor from the Wilson model fitted to the experimental vapor-liquid equilibrium data set by Sazonov[40]. (b) Fick diffusion coefficient. Simulation results (green symbols) are compared with experimental data (+) from the literature[94–96]. (c) Intra-diffusion coefficients of propan-2-ol (red) and water (blue). (d) Shear viscosity. Simulation results (green symbols) are compared with experimental data (+) from the literature[63]

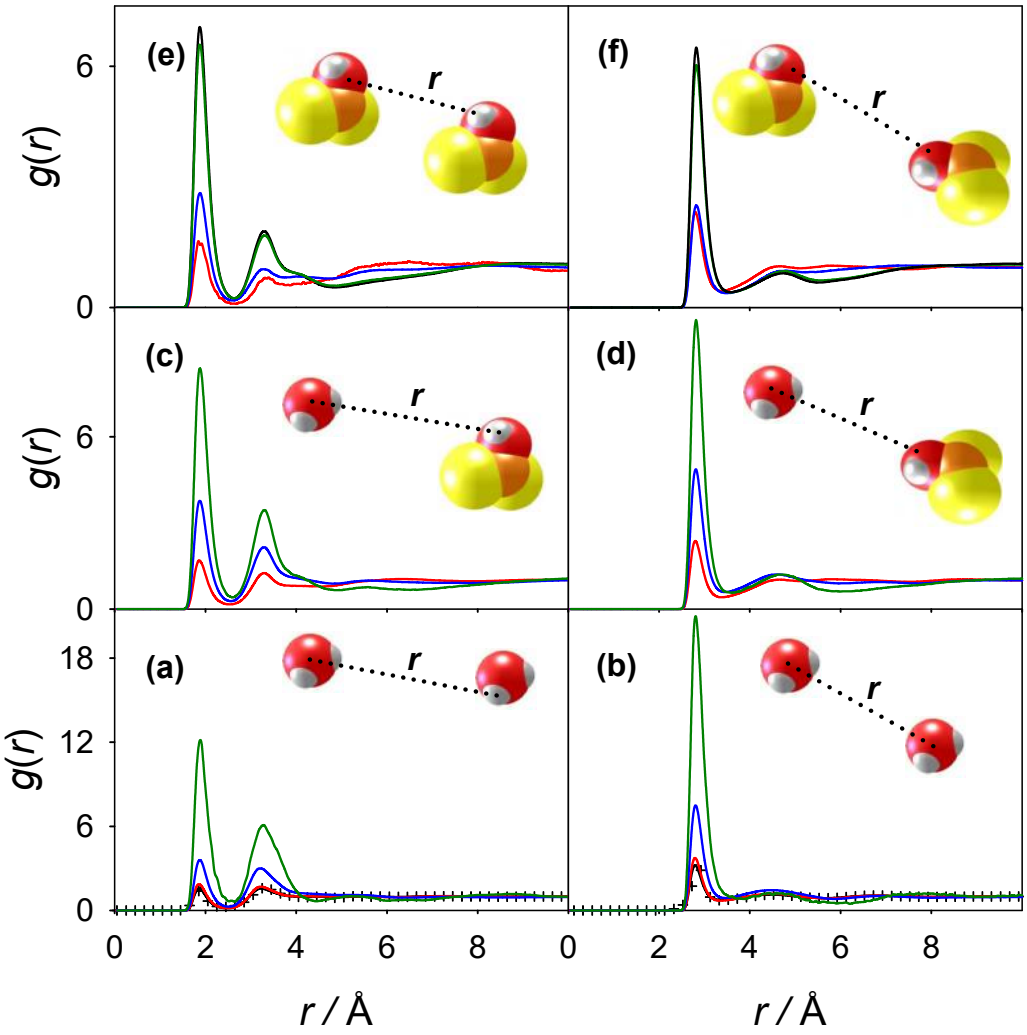


Figure 6: Composition dependence of the radial distribution function for the oxygen-hydrogen (left) and oxygen-oxygen (right) interactions at 298.15 K and 0.1 MPa. Panels (a) and (b) depict water-water pair interactions. Panels (c) and (d) show the unlike water-alcohol pair interactions and panels (e) and (f) the alcohol-alcohol pair interactions. Panels (a) and (b) depict experimental data [103] (+) for pure water at 298.15 K, solid lines are simulation results. Black lines represent the pure substances, different compositions of the mixture are represented by red lines $x_{\mathrm{IPA}} = 0.05$ mol mol$^{-1}$, blue lines $x_{\mathrm{IPA}} = 0.4$ mol mol$^{-1}$ and green lines $x_{\mathrm{IPA}} = 0.95$ mol mol$^{-1}$.

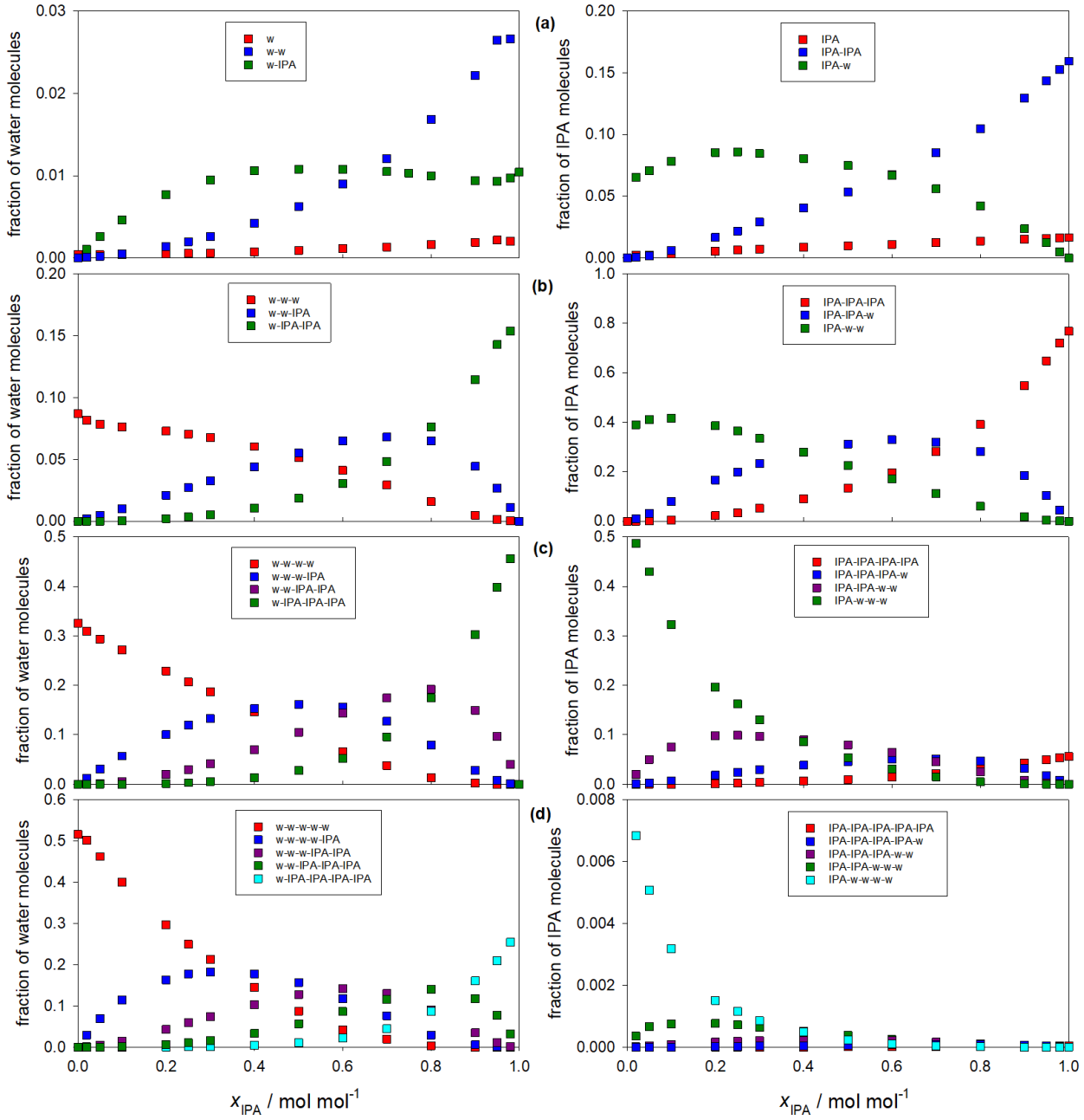


Figure 7: Hydrogen bonding statistics for the aqueous propan-2-ol mixture at 298.15 K and 0.1 MPa. The fractions of water (left) and propan-2-ol (right) molecules with 0 to 1 (a), 2 (b), 3 (c) and 4 (d) hydrogen bonded neighbors are shown, differentiating between cluster composition, where "w" stands for water and "IPA" for propan-2-ol.

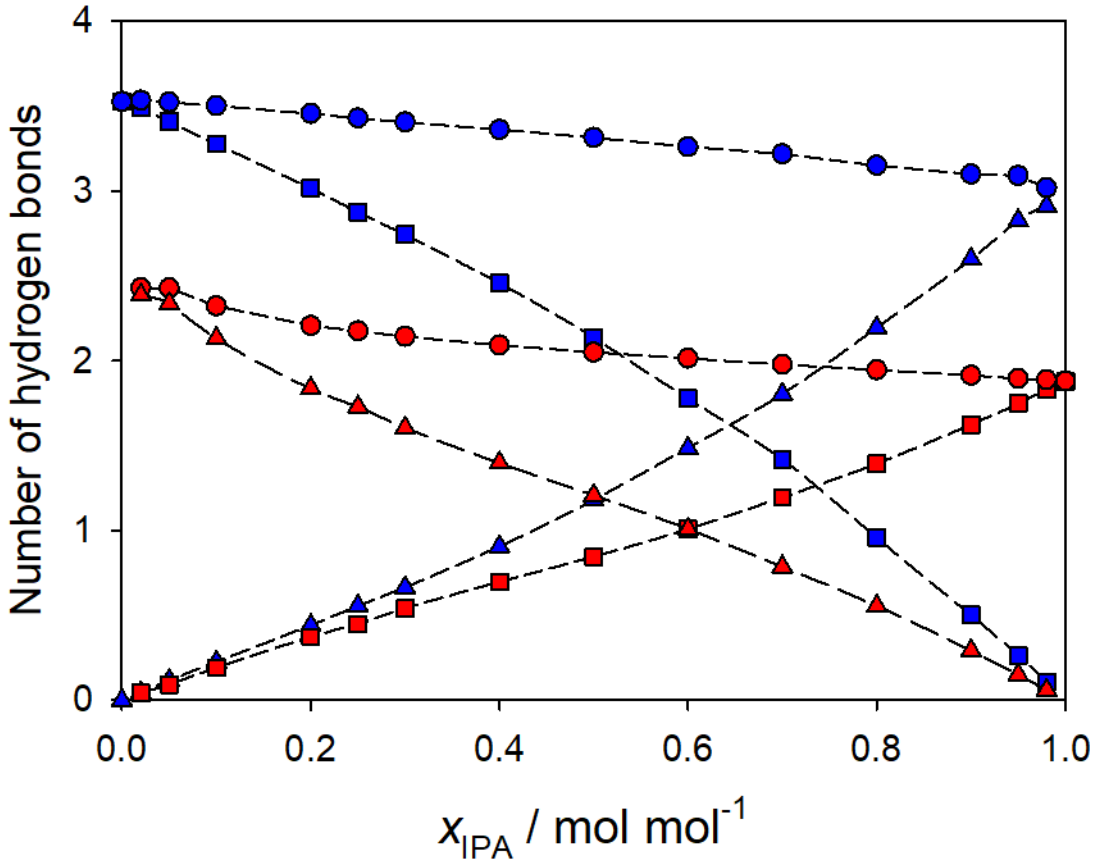


Figure 8: Total number of hydrogen bonds per water (blue symbols) or propan-2-ol (red symbols) molecule at 298.15 K and 0.1 MPa (bullets), differentiating between unlike (water-propan-2-ol) pairs (triangles) and like pairs (squares).

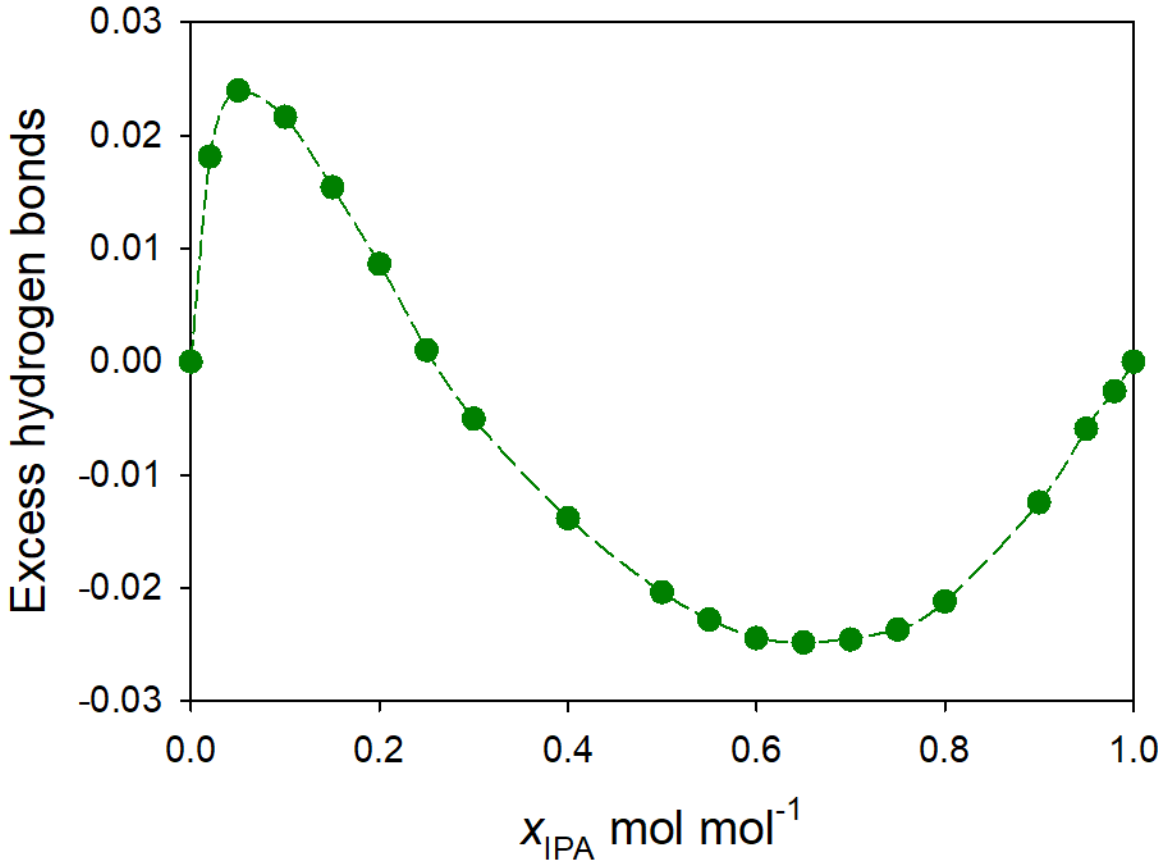


Figure 9: Excess number of hydrogen bonds of propan-2-ol + water at 298.15 K and 0.1 MPa. The dashed line serves as a guide to the eye.

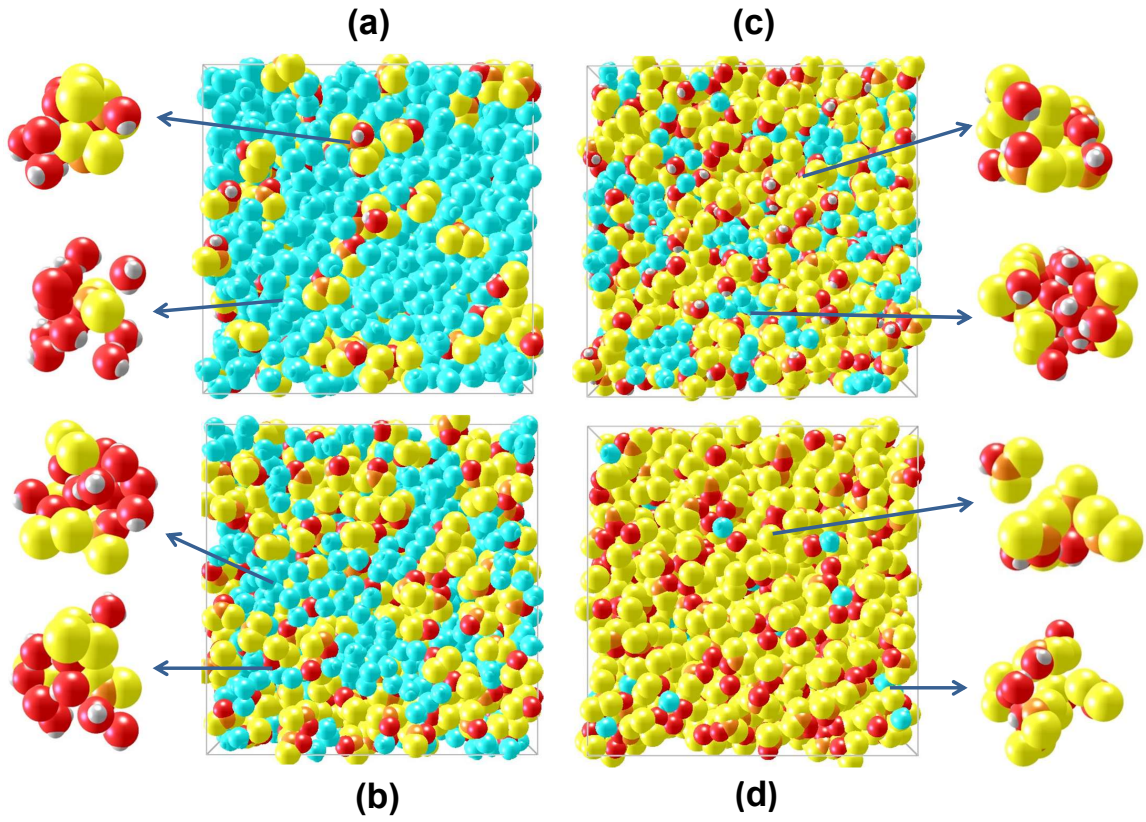


Figure 10: Simulation snapshots and selected spatial molecular configurations of the aqueous propan-2-ol mixture at 298.15 K and 0.1 MPa with $x_{\mathrm{IPA}}$ = 0.1 (a), 0.3 (b), 0.5 (c) and 0.9 mol mol$^{-1}$ (d). Except for the overall snapshots, where the water molecules are colored in blue, oxygen atoms are red, hydroxyl hydrogen atoms are white, methyl groups are yellow and methanetriyl groups are brown.

# Graphical TOC Entry